Distinct Off-Equatorial Zonal Wind Stress and Oceanic Responses for EP- and CP-Type ENSO Events

SHAYNE MCGREGOR,[a,b] DIETMAR DOMMENGET,[a,b] AND SONJA NESKE[a,c]

[a] *School of Earth Atmosphere and Environment, Monash University, Melbourne, Victoria, Australia*
[b] *Centre of Excellence for Climate Extremes, Monash University, Melbourne, Victoria, Australia*
[c] *GEOMAR Helmholtz Centre for Ocean Research Kiel, Kiel, Germany*

(Manuscript received 24 June 2021, in final form 7 October 2021)

ABSTRACT: This study utilizes observations and a series of idealized experiments to explore whether eastern Pacific (EP)- and central Pacific (CP)-type El Niño–Southern Oscillation (ENSO) events produce surface wind stress responses with distinct spatial structures. We find that the meridionally broader sea surface temperatures (SSTs) during CP events lead to zonal wind stresses that are also meridionally broader than those found during EP-type events, leading to differences in the near-equatorial wind stress curl. These wind spatial structure differences create differences in the associated pre- and post-ENSO event WWV response. For instance, the meridionally narrow winds found during EP events have (i) weaker wind stresses along 5°N and 5°S, leading to weaker Ekman-induced pre-event WWV changes; and (ii) stronger near-equatorial wind stress curls that lead to a much larger post-ENSO event WWV changes than during CP events. The latter suggests that, in the framework of the recharge oscillator model, the EP events have stronger coupling between sea surface temperatures (SST) and thermocline (WWV), supporting more clearly the phase transition of ENSO events, and therefore, the oscillating nature of ENSO than CP events. The results suggest that the spatial structure of the SST pattern and the related differences in the wind stress curl, are required along with equatorial wind stress to accurately model the WWV changes during EP- and CP-type ENSO events.

KEYWORDS: El Nino; ENSO; Warm water volume; Wind stress; Wind stress curl

1. Introduction

The tropical Pacific region contains the world's most prominent interannual climate fluctuation: El Niño–Southern Oscillation (ENSO) (e.g., McPhaden et al. 2006). ENSO describes a coupled ocean–atmosphere phenomenon that fluctuates between (i) anomalously warm eastern equatorial Pacific sea surface temperatures (SSTs) that are accompanied by a weakening or a reversal of the overlying trade winds (El Niño), and (ii) anomalously cool eastern equatorial Pacific SSTs that are accompanied by a strengthening of trade winds (La Niña). More than four decades of intense research has tremendously enhanced our understanding of ENSO and its interannual nature (e.g., Timmermann et al. 2019). However, we still have difficulties in unscrambling the subtleties of ENSO's underlying dynamics, and precisely predicting the ENSO state seasons in advance (Timmermann et al. 2019; e.g., Santoso et al. 2019). Enhancing the predictability of ENSO, which is at least partially reliant on an enhanced understanding of its dynamics, is sought after due to the huge impact these events have on societies around the globe through their modulation of severe weather events and climatic conditions (e.g., Diaz et al. 2002; McPhaden et al. 2006; Taschetto et al. 2020; Sprintall et al. 2020; Goddard and Gershunov 2020).

Traditional conceptual models of ENSO highlight our understanding of this phenomenon by summarizing the important mechanisms and feedbacks known at the time of their development (Suarez and Schopf 1988; Weisberg and Wang 1997; Picaut et al. 1997; Jin 1997; Summarized by Wang and Picaut 2004). One of the leading conceptual models for ENSO's apparent oscillatory behavior is Jin's (1997) recharge–discharge oscillator (RDO) theory. This theory suggests that the surface zonal wind/SST anomaly (SSTA) feedback that underpins El Niño (La Niña) event growth, generates an oceanic (Sverdrup type) response that discharges (recharges) equatorial upper ocean heat, conditioning the system for a change in phase of ENSO (see also Wang and Picaut (2004) for comprehensive description of the RDO theory). We note here that the upper ocean heat content of the tropical Pacific is typically measured observationally by the warm water volume (WWV), which is the thermocline depth integrated over 120°E–80°W, 5°N–5°S (Meinen and McPhaden 2000). Jin's (1997) theory has largely been confirmed by observational studies which show that the WWV leads ENSO SST by 1–3 seasons (Meinen and McPhaden 2000; Meinen and Mcphaden 2001; McPhaden 2012; Bunge and Clarke 2014). Consequently, tropical Pacific WWV is seen as a precursor to ENSO events and is largely considered to underlie their predictability.

While the value of these conceptual models cannot be questioned, it has become increasingly apparent that there are many complexities of ENSO events that are not explicitly considered by these conceptual models. For example, the existence of different ENSO types: central Pacific (CP, with maximum SST anomaly found in the central equatorial Pacific) versus eastern Pacific (EP, with maximum SST anomaly found in the eastern equatorial Pacific) ENSO events (Kao and Yu 2009; Kug et al. 2009; McPhaden et al. 2011).

Corresponding author: Shayne McGregor, shayne.mcgregor@monash.edu

DOI: 10.1175/JCLI-D-21-0473.1

One of these key simplifications in conceptual ENSO models is that the SST growth rate and coupling to the thermocline (WWV) are a function of the equatorial wind stress only (Jin 1997; Burgers et al. 2005; Clarke et al. 2007). This simplification, which neglects the wind stress curl that drives the slower adjusted (Sverdrup) oceanic response, is akin to making an assumption that the anomalous winds accompanying all ENSO events can be represented by a single pattern. Similar assumptions were initially made about SSTA patterns of ENSO events, despite it being previously recognized from very early analysis that no two El Niño events appear to be exactly the same (e.g., Wyrtki 1975). However, since the early 2000s the community has attempted to more systematically classify ENSO event diversity (Capotondi et al. 2015, 2020).

This simplification around the structure of winds is potentially important as the zonal extent and longitude of the zonal wind maximum differences during CP and EP El Niño events have been related to event duration differences (Kug et al. 2009, 2010), while the meridional extent of ENSOs equatorial zonal wind stresses has been related to the frequency of events (Kirtman 1997; Capotondi et al. 2006). In general, models found to display ENSO zonal wind stresses that have a narrow meridional extent and a related strong near-equatorial wind stress curl, were more likely to display ENSO events that occur too frequently (Capotondi et al. 2006). The recent study of Im et al. (2015) has also suggested that ENSO phase asymmetries in the meridional extent of the zonal wind stresses may play some role in their duration asymmetry.

The recent study of Neske et al. (2021) suggests that EP El Niño–type SSTAs tend to have zonal wind stress anomalies that have a narrower meridional extent and stronger near-equatorial wind stress curl than CP-type events. Furthermore, their results suggested that EP-type ENSO events typically had a strong adjusted WWV response, while CP events typically displayed a weak adjusted WWV response. We note here that the adjusted WWV response refers to the WWV response after oceanic adjustment and can often be thought of as the post-ENSO event WWV. The results of Neske et al. (2021) are broadly consistent with earlier studies (Kug et al. 2009, 2010; Singh and Delcroix 2013), which show a much weaker post-ENSO event WWV discharge occurring for CP-type ENSO events than for EP-type ENSO events. The post-ENSO event WWV is incredibly important as conceptual models suggest that it is the beginning of a new ENSO event of the opposite sign in the following boreal winter (e.g., Jin 1997). However, the fact that the relationship between SST and wind is complex and nonlinear (Frauen and Dommenget 2010; Dommenget et al. 2013; DiNezio and Deser 2014; Izumo et al. 2019), led Neske et al. (2021) to conclude that further numerical experiments were needed in order to identify the role of SST spatial structure (EP/CP ENSO events) on the resulting winds.

While El Niño event diversity has been actively investigated for some time, studies reporting on differences in the surface wind response have largely focused on the zonal extent and longitude of the anomalous zonal wind stress maximum (e.g., Kug et al. 2009). Thus, in this paper we utilize a series of idealized uncoupled experiments to thoroughly explore the role SSTA structure and location play modulating the meridional extent of the surface winds and the resulting oceanic response. We also assess the validity of the assumption utilized in conceptual ENSO models that differences in the wind stress patterns can be represented by the magnitude of equatorial Pacific wind stresses alone, neglecting an explicit presentation of wind stress curl. AGCM experiments are carried out to estimate the wind stress response to prescribed idealized SSTA patterns, while simple ocean model simulations are used to estimate the WWV response resulting from the modeled wind stresses. Observational data are then analyzed to ground truth the experiment results. These experiments along with the observational datasets utilized in this study are described in section 2. Section 3 details the results of the AGCM experiments, while section 4 details the results of the simple ocean model simulations. Discussion and conclusions are presented in section 5.

2. Data, models, and experiments

Section 2a briefly details the observational data utilized here. Details of the idealized SSTA forcing, the atmospheric model and its simulations, along with the simple ocean model simulations, follow in sections 2b, 2c, and 2d, respectively.

a. Observational data

The HADISST SST dataset, extending from 1950 to 2020, is utilized throughout this study (Rayner et al. 2003). Prior to any analysis taking place, the SSTs were linearly detrended throughout the entire period. Anomalies of SST were calculated by removing the long-term climatology from the 1950–2010 period.

Monthly mean 10-m surface wind data from the European Centre for Medium-Range Weather Forecasts (ERA-Interim) (Dee and Uppala 2009) product are used over the 1980–2015 period. These winds were first converted to wind stresses before the long-term seasonal cycle and linear trend were removed. Wind stresses were calculated using the quadratic stress law that is detailed in McGregor et al. (2013b).

Gridded estimates of observed Pacific upper ocean temperatures, calculated from observed in situ temperature profiles for the 1980–2015 period (Smith 1995), are used in the calculation of the observed WWV (Meinen and McPhaden 2000). As introduced above, WWV is defined as the volume of water with temperature above 20°C in the equatorial Pacific (5°N–5°S, 120°E–80°W). [Further details of the WWV are available in Meinen and McPhaden (2000) and at https://www.pmel.noaa.gov/tao/wwv/data/.]

b. Idealized SSTA forcing

Here, we will define the various flavors of ENSO SSTA (Capotondi et al. 2015) using the rotated empirical orthogonal function (EOF) analysis methodology of Dommenget et al. (2013). Both Takahashi et al. (2011) and Dommenget et al. (2013) identified that the first two EOFs of tropical Pacific SSTA [see Figs. 1a and 1b of Dommenget et al. (2013)] are actually nonlinearly related, such that the magnitude of the

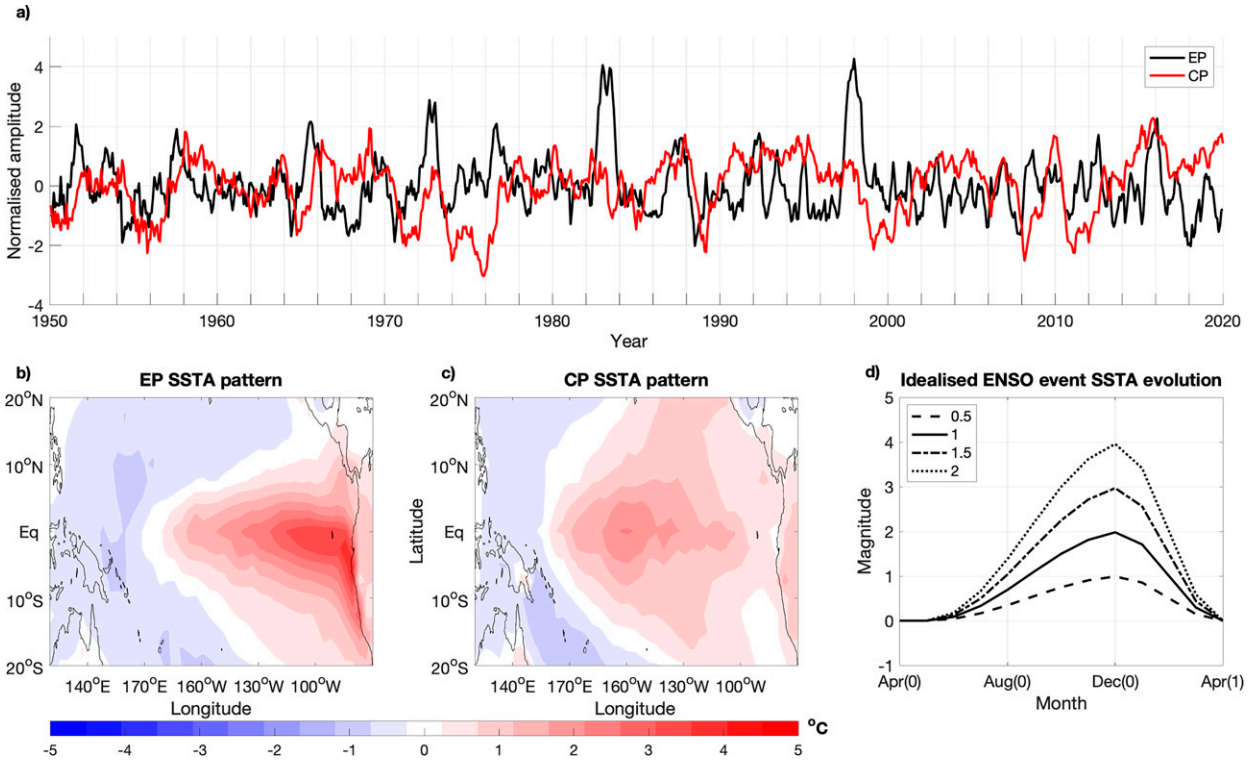

FIG. 1. (a) Principle components (PCs) for the EP and CP modes, whose (b),(c) spatial patterns are shown. (d) The solid line displays the idealized time series used to force the AGCM experiments, while the different magnitudes utilized are displayed by various line types (see legend).

first principle component (PC) time series can provide information about the second PC times series. To identify two PCs that are orthogonal, they normalized and rotated the two PCs counter clockwise by 45° (Dommenget et al. 2013). The resulting PCs were named the PC_{El_Nino} and PC_{La_Nina}, but can also be thought of as PC_{EP} and PC_{CP}, as proposed by Takahashi et al. (2011), given that most La Niña events are CP type. Here, we will utilize the Takahashi et al. (2011) notation as our main concern is on the spatial structure of the SSTA, rather than their typical sign (Fig. 1a). The associated rotated EOFs are presented in Figs. 1b and c, and we note that both patterns have the same Niño-3.4 region SSTA (190°E–120°W, 5°S–5°N; hereafter Niño-3.4) magnitude.

c. *Atmospheric model and experiments*

The atmosphere general circulation model (AGCM) utilized here is a low resolution version of Australian Community Climate and Earth System Simulator (ACCESS) model (Bi et al. 2013), which is based around the Met Office (UKMO) Unified Model atmospheric GCM with Hadley Centre Global Environment Model version 2 (HadGEM2) physics (Davies et al. 2005; Martin et al. 2010, 2011). It is configured to run at a horizontal grid spacing of 3.75° longitude by 2.58° latitude with 38 vertical atmosphere levels (Frauen et al. 2014).

We carry out a series of AGCM simulation to explore surface wind stress differences in the atmospheric response to EP and CP events (Figs. 1b,c). Each simulation was run for 25 years, and the difference between the simulations was in the underlying/forcing SSTs, which in most cases included SST anomalies (SSTA) superimposed onto the climatology (1950–2010). The superimposed SSTAs have a fixed pattern that is based on either the CP (Fig. 1b) or EP (Fig. 1c) event patterns (see section 2a), or a combination of both (Fig. 2), depending on the experiment details. In all cases the added SSTA temporally evolves with an annually repeating idealized evolution that approximates the apparent synchronization of ENSO events to the seasonal cycle (Fig. 1d). These experiments effectively explore the parameter space of EP and CP events, where the amplitude of this idealized temporal evolution is scaled such that it spans the EP and CP range between ±2, in increments of 0.5 (81 experiments in total). This parameter space explored appears to be largely covered by the observational EP and CP time series displayed in Fig. 1a. The center panel of Fig. 2 displays the peak (October–February average) Niño-3.4 SSTAs for each of the 81 AGCM experiments, while the outer panels provide examples of the different spatial structures and amplitudes of SSTA forcing utilized.

We note that experiment anomalies analyzed here and elsewhere in this manuscript are calculated by differencing with the climatological simulation (EP = 0 and CP = 0) output.

d. *Ocean model and experiments*

A linear 1.5-layer shallow water anomaly model (SWM) with 1° horizontal grid spacing is utilized to understand how

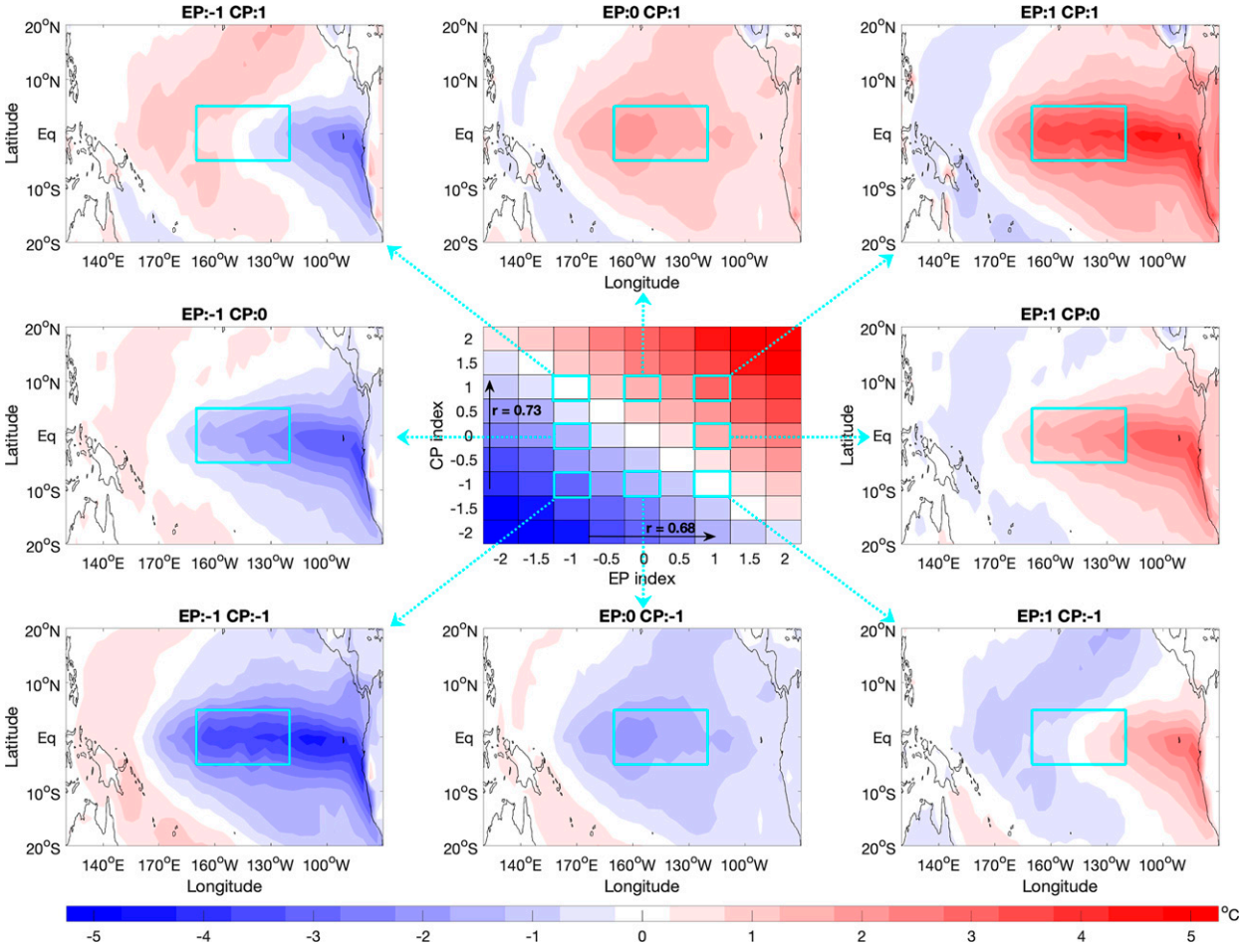

FIG. 2. Outer panels display the peak (October–February average) SSTA (°C) during the ENSO event, for eight specific values of the EP and CP indices (see panel titles). The center panel displays the peak central Pacific (Niño-3.4 region) SSTA (°C) for each simulation, where the *x* and *y* axes denote the EP and CP index value, respectively.

the EP and CP event wind differences influence changes in WWV. Details of the model can be found in Neske and McGregor (2018; their Text S1) and McGregor et al. (2007). It is worth noting here that the SWM, when forced with ERA-Interim surface wind stress anomalies, produces monthly mean WWV changes consistent with those observed, as indicated by a correlation coefficient of 0.86 (Neske et al. 2021).

The SWM is forced with monthly average wind stress anomalies from the AGCM experiments detailed above. However, rather than simply forcing the SWM continuously with AGCM output for the full 25 years for each experiment, the wind stress anomalies are broken into individual years that span from April of the initial year to April of the following year for two main reasons. First, the April–April span covers the full evolution of the applied ENSO event SSTA forcing (Fig. 1d). Second, the separation into individual 13-month periods, which allowed for 24 forced SWM simulations for each AGCM simulation, was carried out as the oceanic adjustment to the wind stress forcing is delayed, and forcing the model continuously acts to obscure the adjusted oceanic response we wanted to analyze. Each of these 24 simulations, which was forced by modeled anomalous wind stresses for 13 months (i.e., from the beginning of April in year 0 to the end of April in year 1), was extended to run for 24 months in total (i.e., to the end of March in year 2) with no wind stress forcing after the 13th month so that the delayed oceanic adjustment could be observed. The resulting experiment pycnocline depth anomalies are averaged over the total WWV region (120°E–80°W, 5°N–5°S), along with its eastern and western components, WWV west region (120°E–150°W, 5°N–5°S), WWV east region (150°–80°W, 5°N–5°S), to obtain regional average WWV anomalies.

3. The surface wind stress response to EP and CP events

a. Modeled EP/CP event zonal wind stress differences

In this section we explore the zonal surface winds resulting from the AGCM experiments described in section 2c. Peak-ENSO event equatorial zonal wind stress anomalies, which are calculated as the average zonal wind stress between

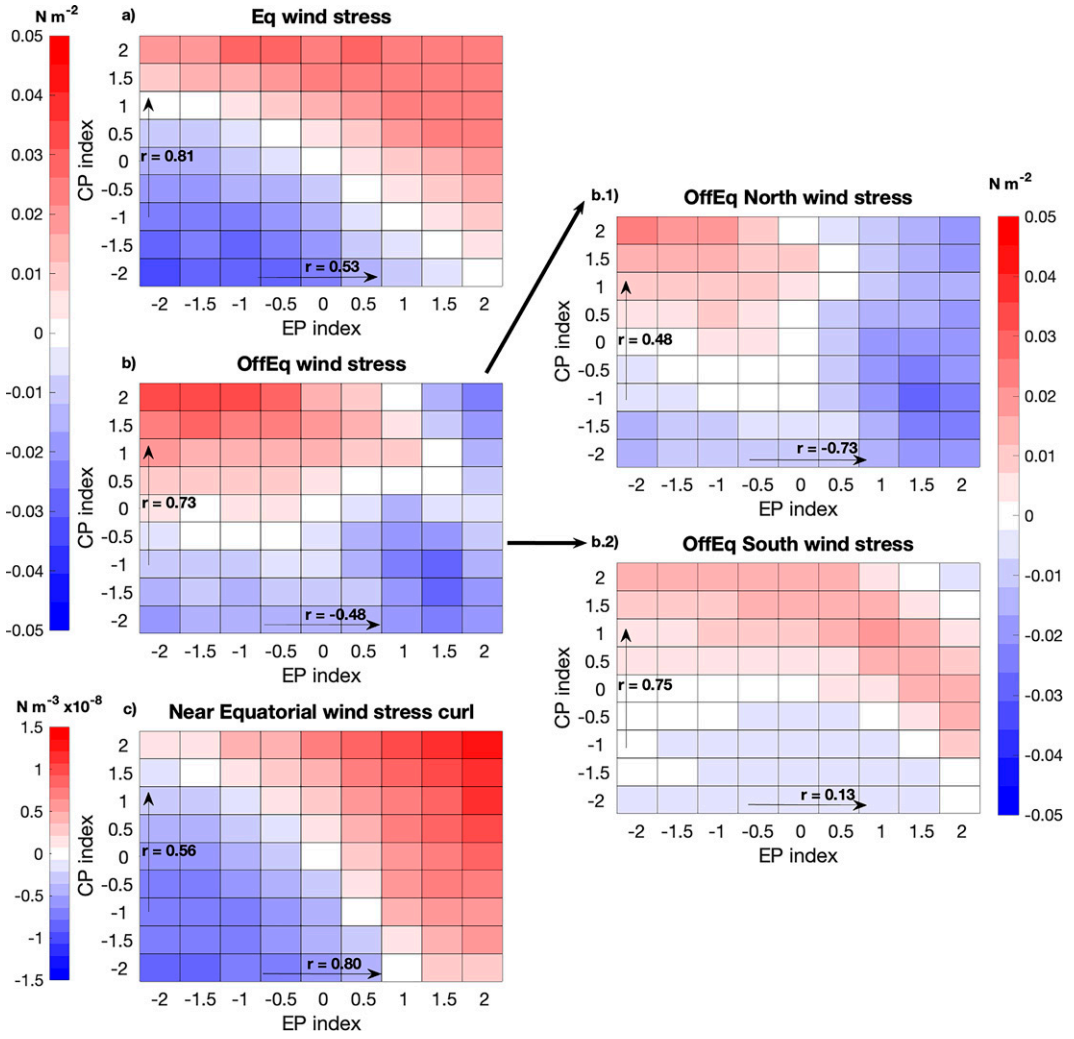

FIG. 3. Peak-ENSO event (October–February average) zonal wind stress anomaly for the (a) equatorial region (5°S–5°N, 140°E–100°W); (b) off-equatorial region, which is the sum of wind stress in the Northern Hemisphere region (5°–10°N, 140°E–100°W) and Southern Hemisphere region (10°–5°S, 140°E–100°W); and (c) the near-equatorial wind stress curl, which is the difference of wind stress curls in the Northern Hemisphere region (2°–8°N, 140°E–100°W) and Southern Hemisphere region (8°–2°S, 140°E–100°W). The off-equatorial region wind stresses from the (b.1) northern and (b.2) southern regions are displayed.

5°S–5°N and 140°E–100°W of all 25 simulation years during October–February, are strongly modulated by Niño-3.4 region SSTAs during the same period ($r = 0.95$). This is evidenced by the similarity between Fig. 2 (center panel) and Fig. 3a.

These peak-ENSO equatorial zonal wind stresses also appear to be modulated by both CP events and EP events, as is evidenced in Fig. 3a by the transitions from strong negative values in the bottom-left corner, toward positive values in the top-left corner and bottom-right corner, respectively. However, CP events play a stronger modulating role ($r = 0.81$) than EP events, which only display a correlation coefficient (r) of 0.53, evidenced by a slight anticlockwise rotation of the wind stresses (Fig. 3a) relative to the SSTA (Fig. 2, center). Wind stresses in the western half of the equatorial region (140°E–160°W) are largely modulated by CP events ($r = 0.96$; EP events only play a minor role $r = 0.10$), while winds in the eastern half of the region (160°–100°W) are largely modulated by EP events ($r = 0.98$; CP events play a minor role $r = 0.10$). As to why the CP play a more prominent role, the western Pacific region wind stresses have a larger standard deviation ($\sigma = 0.0059$ N m^{-2}) than the eastern Pacific ($\sigma = 0.0012$ N m^{-2}). This fact is also reflected by the regression slope (b) of 0.0213 N m^{-2}, calculated between the CP events and western equatorial Pacific zonal wind stresses, which is much larger than that calculated between the EP events and zonal wind stresses in the eastern equatorial Pacific ($b = 0.0124$ N m^{-2}). The prominent role of SSTAs in the central/western Pacific is consistent with idealized AGCM experiments of Taschetto et al. (2016a, 2020), who identify that the region around the date line (where CP El Niño warming is located) produces

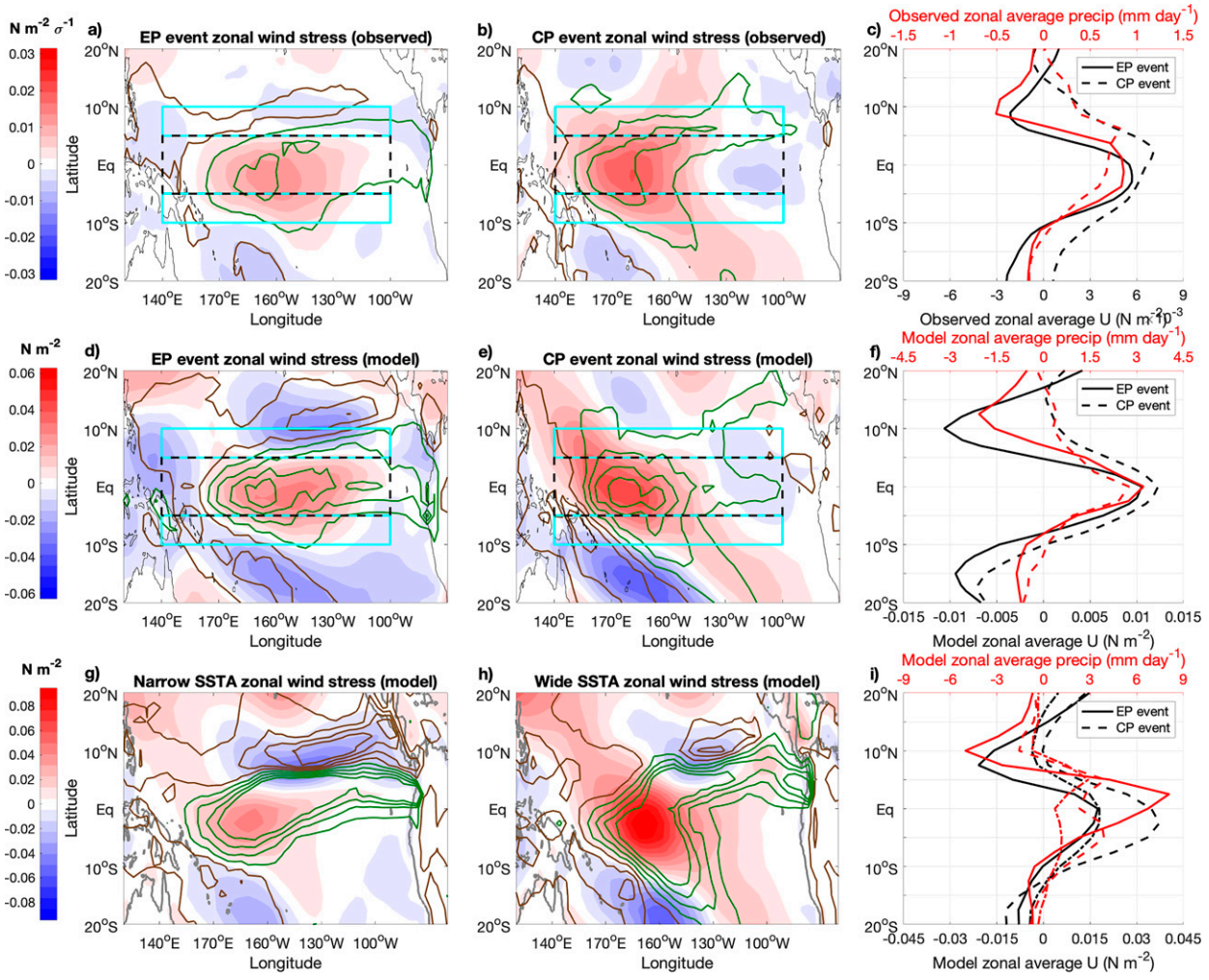

FIG. 4. The observed (a) EP and (b) CP ENSO event surface wind stress (shading; N m^{-2} per standard deviation) and precipitation (contours; mm day^{-1} per standard deviation) response, which is calculated as the regression of observed surface wind stress onto the EP and CP event indices. The modeled linear (d) EP and (e) CP ENSO event surface zonal wind stress (shading) and precipitation (contours) response is displayed, which is calculated as half the composite difference between peak (October–February) surface wind stress with positive (El Niño) and negative (La Niña) EP (EP index > 0 minus EP index < 0 for all CP index values) and CP (CP index > 0 minus CP index < 0 for all EP index values) event indices, respectively. The modeled linear (g) EP and (h) CP ENSO event surface zonal wind stress (shading) and precipitation (contours) response for the idealized narrow and wide SSTA experiments. In (a), (b), (d), and (e), the inset cyan regions indicate off-equatorial regions, while dashed back regions indicate the equatorial region. (c),(f),(i) The zonal average zonal wind stress (black) and precipitation (red) response between 140°E and 100°W seen in two panels to the left on each row. Dashed lines are for the CP-type (meridionally wide) events, while solid black lines are for the EP-type (meridionally narrow) events.

the strongest atmospheric response in the Pacific compared to the eastern and western Pacific regions.

Off-equatorial zonal wind stress, which is calculated as the sum of average zonal wind stress in the north (5°–10°N, 140°E–100°W) and south (5°–10°S, 140°E–100°W) off-equatorial regions, presents a more complex pattern (Fig. 3b) that displays maximums in the top left corner and minimums in the bottom right corner. This indicates that CP and EP SST patterns force very different off-equatorial zonal wind stresses, which is quantified by the correlations that having opposite signs. CP events display a strong positive correlation with the off-equatorial zonal wind stresses ($r = 0.73$), which suggests that CP events typically have surface zonal wind stress response is meridionally broad when combined with their strong positive correlation with equatorial zonal wind stress. EP events on the other hand, display a reasonably strong negative correlation with off-equatorial zonal wind stresses ($r = -0.48$). When this negative off-equatorial zonal wind stress correlation is combined with the strong positive correlation between EP event and equatorial zonal wind stress, it suggests that the surface zonal wind response to EP events are typically relatively narrow, meridionally. These differences in the meridional width of the zonal wind stress responses to CP and EP event SSTA are clearly shown in Figs. 4d–f.

Separating the off-equatorial wind stress into its northern and southern components helps aid the interpretation of the complex relationship with EP and CP event type (Figs. 3b.1,b.2). What becomes apparent is that off-equatorial winds in the northern box are strongly linearly negatively correlated to EP event magnitude ($r = -0.73$), while the off-equatorial winds in the southern box have no significant relationship with EP event magnitude. Both of these relationships show that the anomalous surface zonal wind stress/SSTA feedback of EP events is quite well constrained to the equator, though wind stress curls are enhanced at the northern boundary due to a sharper wind transition. CP event magnitude, on the other hand, has a moderate positive relationship with wind stresses in the northern ($r = 0.48$) and southern ($r = 0.75$) boxes.

Here, rather than focusing on the curl of the horizontal wind stress, which is defined as $\text{curl}(\tau) = \partial\tau_y\partial x - \partial\tau_x\partial y$, we focus on the zonal component of wind stress curl (hereafter referred to as the zonal wind stress curl) by neglecting the first term of the wind stress curl equation. This simplification is carried out as the north–south scale of the wind in the equatorial region is typically much smaller than the east–west scale (e.g., Clarke 2008), suggesting that the first term of the wind stress curl is normally small. We focus on wind stress curl here as it plays an important role in the driving thermocline depth changes off the equator, via Ekman pumping (Qiu and Chen 2010), while the related geostrophic transports can drive WWV changes (Jin 1997). For instance, the positive (negative) wind stress curls found in the northern (southern) off-equatorial Pacific during an El Niño event lead to Ekman divergence in these regions, which raises the underlying thermocline depths generating upwelling westward propagating Rossby waves, these Rossby waves enhance the zonal tilt of the thermocline and lead to a stronger geostrophic discharge of WWV when they impinge on the western boundary. Thus, here we define near-equatorial zonal wind stress curl (Fig. 3c) as the difference between the average zonal wind stress curl in the north (2°–8°N, 140°–260°E) and south (2°–8°S, 140°–260°E) near-equatorial regions.

Figure 3c suggests that near-equatorial wind stress curl appears to be strongly modulated by EP events ($r = 0.80$). This strong relationship between zonal wind stress curl and EP event magnitude is consistent with the correlations reported above, whereby EP event magnitude displays a positive correlation with equatorial zonal wind stresses which transitions sharply to a negative or near-zero correlation in the off-equatorial regions. Taking into account the north–south separation of off-equatorial wind stresses shown in Figs. 3b.1 and 3b.2, this strong relationship between EP event magnitude and wind stress curl is underpinned by the strong negative correlation between EP event magnitude and wind stress in the northern off-equatorial boxed region. This is consistent with expectations given that spatial structure of ENSO winds typically has a more gradual decay to the south than the north (Figs. 4d–f).

The weaker correlation between the CP event index and zonal wind stress curl ($r = 0.56$, Fig. 3c) is consistent with both equatorial and off-equatorial zonal winds having a positive correlation with CP events, as this acts to weaken the associated curl signature. This is also in agreement with the fact that the zonal wind stresses of these events are meridionally broader than those of EP events (Figs. 4d–f). The separation of off-equatorial wind stresses into its north and south components (Figs. 3b.1,b.2), reveals moderate-to-strong relationships between the CP event index and wind stresses in the northern off-equatorial boxed region, and a strong relationship between CP event index and wind stresses in the southern off-equatorial boxed region. Thus, indicating that the positive relationship between CP event magnitude and off-equatorial wind stresses, along with the weak relationship to wind stress curl, is due to the equatorial winds typically having a larger poleward extension in both hemispheres during CP events than that seen in EP events.

b. *Observational verification of EP/CP event zonal wind stress differences*

In this section we detail similarities and differences between the observed and modeled relationships between Pacific zonal wind stresses and the EP and CP event indices. Indices of EP and CP events are those presented in Fig. 1a, while those of observed zonal wind stress are calculated from ERA-Interim 10-m winds (see section 2a). We show that many features of the relationship between EP and CP events and the surface zonal wind stress identified in our idealized model experiments presented in section 3a, are also apparent in these observations.

First, as expected, equatorial zonal wind stresses are clearly modulated by both CP events and EP events, as is evidenced in Fig. 5a by the transitions from strong negative values in the bottom left-hand corner, to strong positive values in the top right-hand corner. Consistent with our idealized model experiments, CP events also appear to play a stronger modulating role of equatorial zonal wind stresses than EP events, as they display a larger correlation ($r = 0.58$) than that found for EP events ($r = 0.45$). Again, this result is broadly consistent with earlier studies that show a stronger atmospheric response to date line region SSTAs (where CP El Niño warming is located) when compared to other regions of the equatorial Pacific (Taschetto et al. 2016b, 2020).

Second, the observed off-equatorial zonal wind stresses have a moderate positive correlation with the CP event index ($r = 0.45$). The EP event index, on the other hand, has very little role modulating the observed off-equatorial zonal wind stresses ($r = 0.09$; Fig. 5b). Both, our modeled and the observed zonal wind stress response, suggest that CP events display a surface zonal wind stress response that is meridionally broad (consistent with the positive correlations between the CP index and both, equatorial and off-equatorial zonal wind stress), while EP events display a zonal wind stress response that is meridionally narrow in comparison (consistent with the positive correlations between the EP index and equatorial zonal wind stress, and the negative or near-zero correlations between the EP index and off-equatorial zonal wind stress). However, where the idealized experiments differ most from those observed, is the relationship between the EP

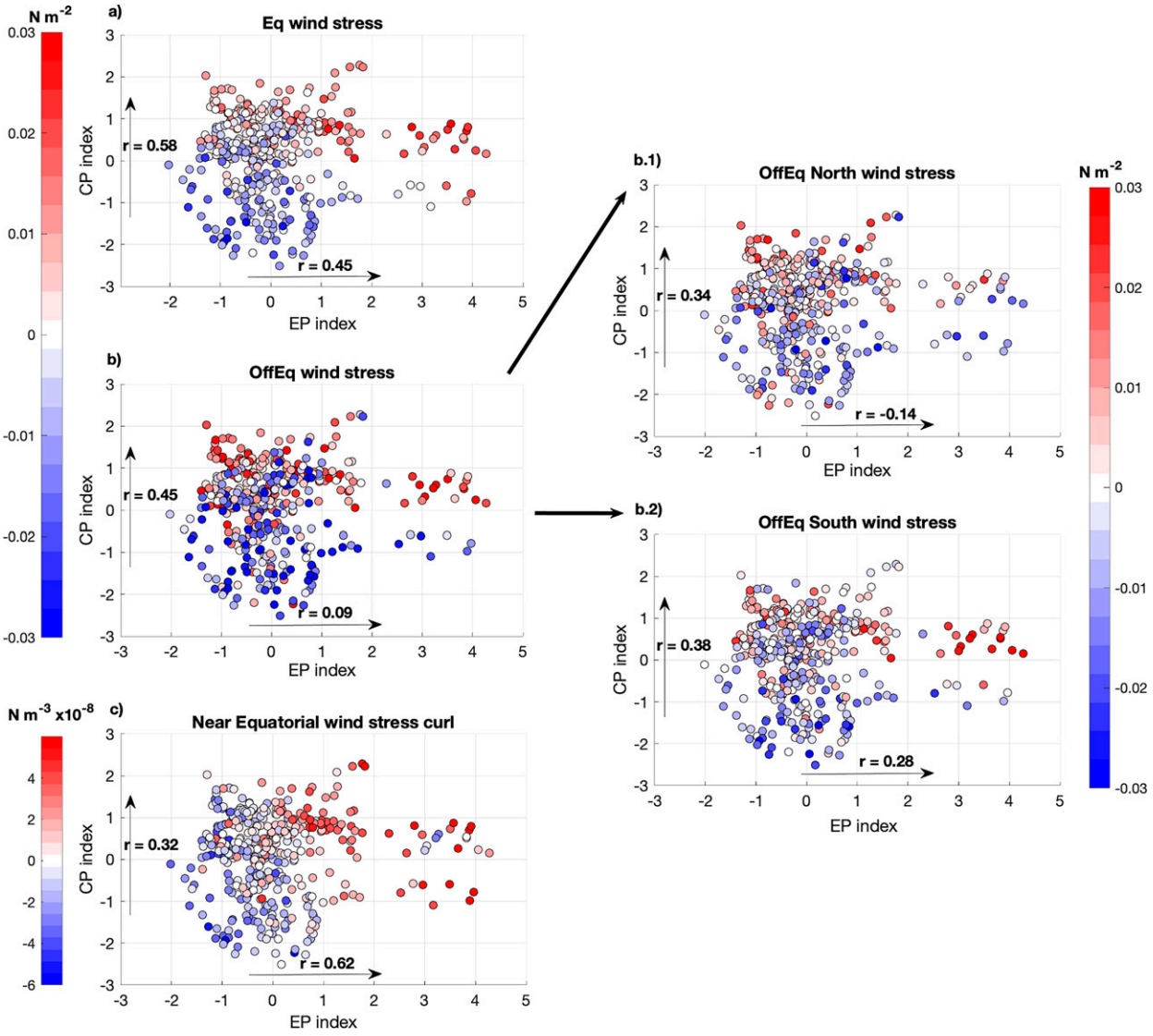

FIG. 5. Observed ENSO event zonal wind stress anomaly for the (a) equatorial region (5°S–5°N, 140°E–100°W); (b) off-equatorial region, which is the sum of wind stress in the Northern Hemisphere region (5°–10°N, 140°E–100°W) and Southern Hemisphere region (10°–5°S, 140°E–100°W); while (c) the near-equatorial wind stress curl, which is the sum of wind stress curls in the Northern Hemisphere region (2°–8°N, 140°E–100°W) and Southern Hemisphere region (8°–2°S, 140°E–100°W) is presented. The off-equatorial region wind stresses from the (b.1) northern and (b.2) southern regions are displayed.

index and off-equatorial wind stresses. The idealized model experiments show a moderate negative correlation, while the observed relationship is near zero (Figs. 3b and 5b). Separating the impact of both hemispheres on this relationship difference, differences are apparent in the SH, as the CP event modulation is weaker in the observations than that produced by the idealized experiments, while the EP event modulation is stronger in the observations than that produced by the idealized experiments (Figs. 3b.2 and 5b.2). It is also clear that the differences between the modeled and observed relationship (within ±10° latitude) lie most prominently in the NH as the idealized model experiments show a strong negative zonal wind stress response (Fig. 3b.1), while the observed wind response in this region is much weaker (Fig. 5b.1).

Comparing the spatial patterns of the modeled and observed zonal wind response (Figs. 4a,d), reveals that (i) the model produces opposing off-equatorial surface zonal winds south and north of the equatorial response that is almost as strong as the modeled equatorial response; and (ii) that this modeled off-equatorial response is much larger than that seen in the observations, which appears to show a zonal wind response which is less than half the magnitude of the observed equatorial response. This model enhanced off-equatorial zonal wind response could be related to background state biases, a bias in the anomalous response to the imposed

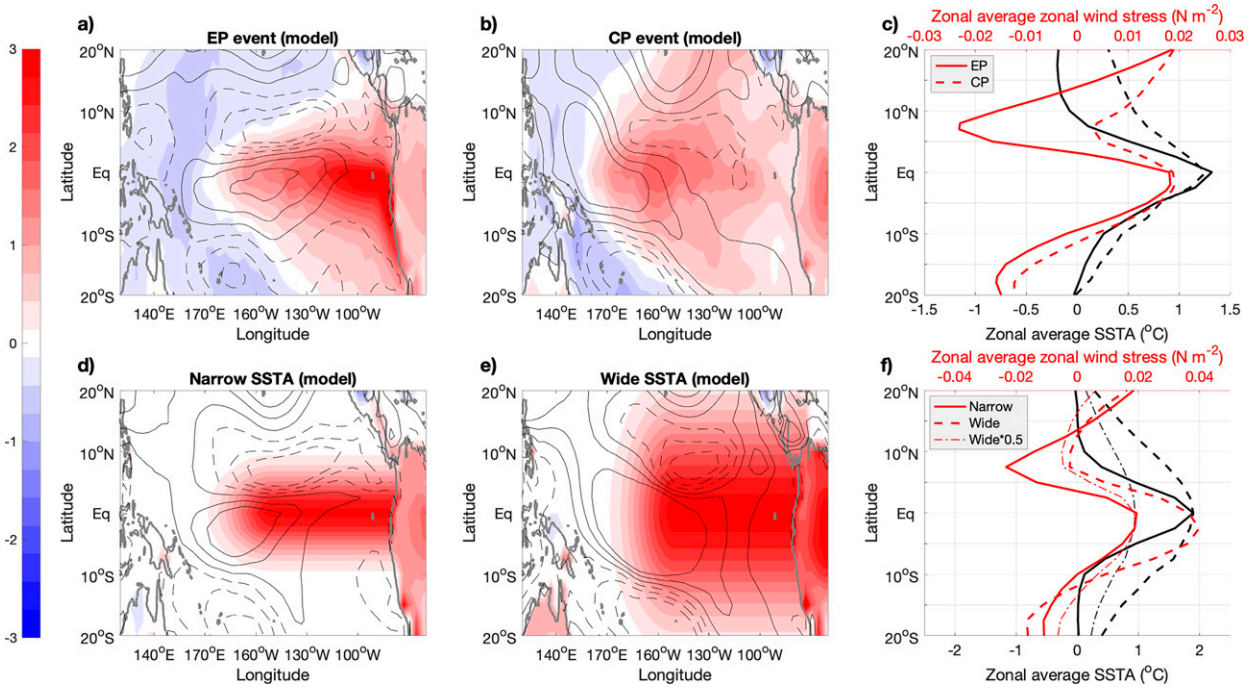

FIG. 6. The modeled linear (a) EP and (b) CP ENSO event SSTA (shading) and surface zonal wind stress response (contours), which is calculated as half of the composite difference (used to represent the linear response) between peak (October–February) surface wind stress with positive (El Niño) and negative (La Niña) EP and CP event indices, respectively. The idealized meridionally (d) narrow and (e) broad ENSO event SSTA (shading) and surface zonal wind stress response (contours). (c) The zonal average SSTA (black lines) and zonal wind stress (red lines) response between 140°E and 100°W for EP (solid lines) and CP (dashed lines) events, respectively. (f) The zonal average SSTA (black lines) and zonal wind stress (red lines) response between 140°E and 100°W for the meridionally narrow (solid lines) and broad (dashed lines) experiments, respectively.

SSTA forcing, or a combination of both of these. However, at present, it is beyond the scope of the current manuscript to delve further into this topic. Despite the differences raised here being present in both hemispheres, they are only apparent in the defined northern off-equatorial region (Fig. 3b.1) as the zonal equatorial winds transition more quickly to the opposite sign moving northward such that this difference occurs in the northern region.

Finally, the observed zonal wind stress curls of the near-equatorial region (Fig. 5c) have a larger correlation with EP events ($r = 0.62$), than the correlation found with CP events ($r = 0.32$). The stronger near-equatorial curl response for EP events is consistent with the narrower meridional structure of their zonal winds relative to CP events, which is again consistent with the model results (Fig. 3c). Furthermore, these observational and model results suggest that near-equatorial wind stress curl can be viewed as largely a function of EP events alone.

c. *Understanding the EP and CP event zonal wind stress meridional extent differences*

Initial analysis undertaken to better understand why CP ENSO events generate a meridionally broader wind response than EP events reveals that, in the zonal average, CP event SSTAs are meridionally broader than those of EP events (Figs. 6a–c). This meridional extent difference in the SSTAs and zonal wind stresses are most apparent in the NH, but they still exist in the SH (Fig. 6c). There are also differences in EP and CP event SSTAs in the location and magnitude of SSTAs that may play a role in the wind response differences. To isolate only the width of the SSTA, we carried out a further AGCM experiment that followed a similar method to that outlined in section 2c. However, the SSTAs added in these experiments were highly idealized (Figs. 6d,e), such that only the meridional width of the anomaly varied between the experiments (Fig. 6f). As much more energy is available in the experiment with meridionally broad SSTAs, we also experimented with meridionally broad SSTA pattern that had a maximum SSTA that was half the magnitude of the meridionally narrow experiment.

Results of these experiments revealed the experiment with the large SSTA meridional extent, produced a surface zonal wind stress response that also displayed a large meridional extent (Figs. 6d–f). The consistency of the results of these idealized experiments with the EP and CP event experiment results presented in section 3a, suggests that the width of the SSTA is largely responsible for the width of the zonal wind stress response, while the SSTA cooling differences between the EP and CP events between 10° and 20°N plays a relatively minor role (Figs. 6a–c).

Simple atmospheric models suggest that there are two potential pathways that would allow meridionally broader SSTAs to modulate the meridional width of the surface wind

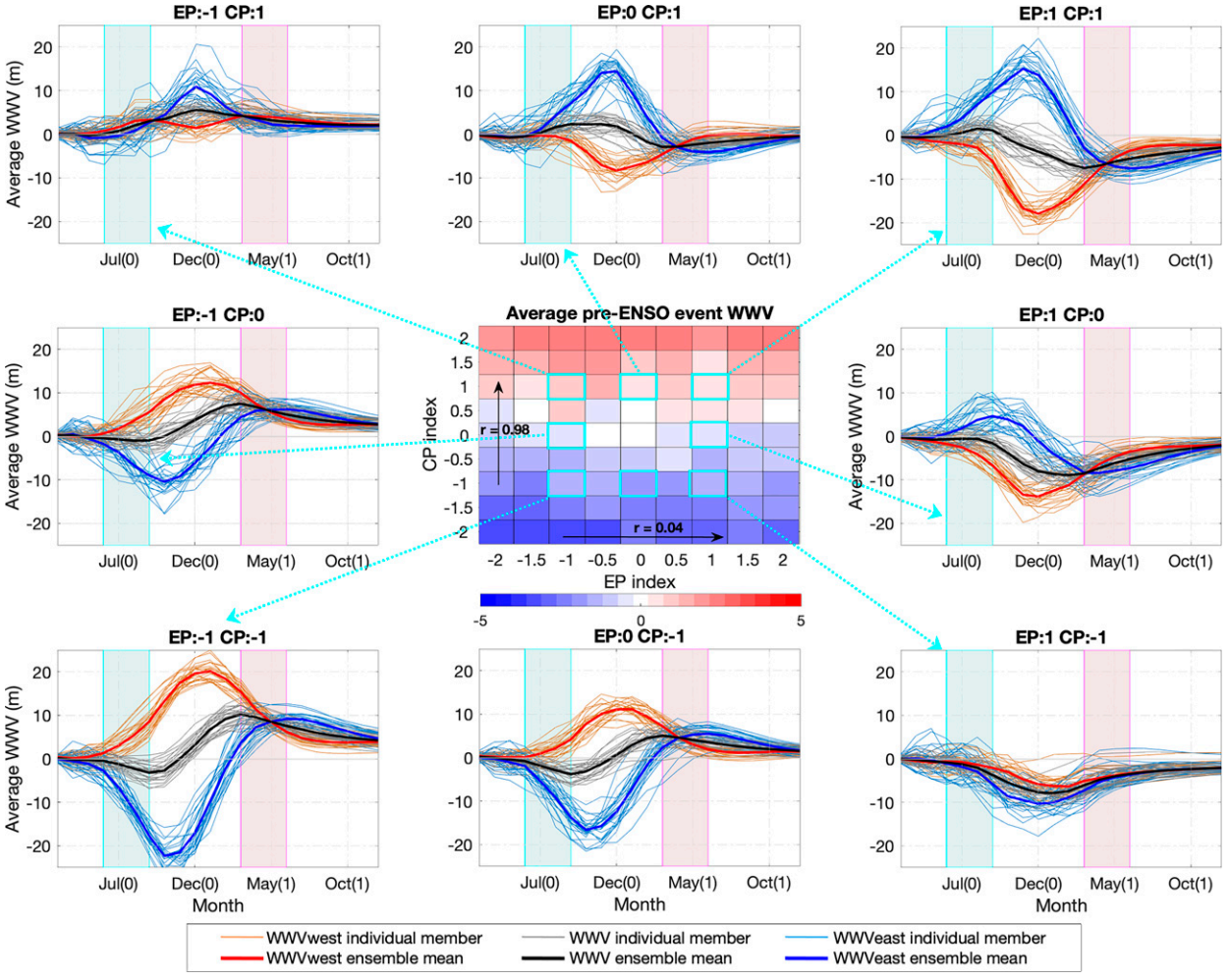

FIG. 7. The center panel displays the pre-ENSO event WWVs for each simulation, where the *x* and *y* axes denote the experiment EP and CP event index, respectively. Outer panels display the total, western, and eastern region WWVs (see legend) during ENSO events, for eight specific EP and CP magnitudes (see panel titles). In each of these outer panels, the light blue region represents the pre-ENSO event period, the pink region represents the post-ENSO event period.

response, and it is possible both of them are working at the same time (e.g., Fu and Wang 1999). First, the broader SSTAs can directly generate a broader wind response as the SSTA forcing directly creates gradients in sea level pressure (Figs. 6d–f) (e.g., Lindzen and Nigam 1987). Second, as the broader SSTAs typically generate a meridionally broader precipitation response, as seen in Figs. 4g–i, the related atmospheric heating anomalies project onto higher-order Rossby waves with a Gill-type atmospheric response (e.g., Gill 1980). Though differences are apparent in the off-equatorial regions of both hemispheres, we also note that the largest wind stress differences between the meridionally narrow and broad SSTA experiments appear between 5° and 10°N. In this region, the strong negative zonal wind anomalies of the meridionally narrow SSTA experiment make way for the small positive zonal wind anomalies of the meridionally broad SSTA experiment. We expect that the EP and CP event differences are largest in this northern off-equatorial region as the EP events seem to produce an equatorward migration of the ITCZ during El Niño events (Figs. 4g,i), while very little migration is apparent in the CP El Niño events (Figs. 4h,i). This equatorward ITCZ migration, which is symbolized by the relatively large negative precipitation anomalies north of ~7°N in the narrow SSTA experiments, is also apparent in the observed and modeled EP event response (Figs. 4a–f).

4. The WWV impact of EP and CP event zonal wind stress meridional extent differences

In this section we aim to develop a better understanding of the pre- and post-ENSO event WWV impact of the EP and CP event zonal wind stress meridional extent differences. The temporal evolution of equatorial Pacific WWVs from our ocean model experiments (see section 2d) are presented in Fig. 7 (outer panels). The focus on WWVs is because existing

literature and conceptual ENSO models suggest that (i) pre-ENSO event buildups (discharges) of WWV are important precursors of El Niño (La Niña) events; while (ii) a WWV discharge (build up) is often the are related to the termination of individual events and the oscillatory nature of ENSO (Jin 1997; Meinen and McPhaden 2000; Burgers et al. 2005).

a. EP/CP-type pre-ENSO event WWV differences

Pre-ENSO event WWV from each of the experiments carried out here (see section 2d), which is defined here as the WWV average during the July–September of the event growth year, can be seen in the center panel of Fig. 7. As the SWM experiments utilized here are set up as a series of discrete events that start from a zero-anomaly state, the potential impact of preceding ENSO events on the pre-ENSO event WWV has been removed (i.e., that a pre–El Niño event WWV buildup is due to slow ocean dynamically induced post event WWV recharge from the preceding La Niña event; e.g., Jin 1997). Thus, the WWV changes seen during the pre-ENSO event period in these simulations can be thought of as a subset of the expected total pre-ENSO event WWV changes. Further to this, we find the modeled pre-event WWV responses are largely a response to meridional Ekman transport, with geostrophic transport typically playing a smaller damping roll (not shown). This is consistent with expectations given the short amount of time from the simulation start up to generate pre-event WWVs along with the relatively small SSTA utilized in the initial 3 months of these simulations (Fig. 1d).

The most striking result of this section is that the pre-event WWV is only a function of the CP index ($r = 0.98$) and is essentially not dependent on the EP index ($r = 0.04$). To understand why, we plot the modeled pre-ENSO event WWV against the modeled anomalous equatorial zonal wind stress, during the same period, revealing a reasonably strong relationship ($r = 0.72$) (Figs. 8a,b). The relationship is relatively weak, however, when compared to the relationship between pre-ENSO event WWV and the anomalous off-equatorial wind stresses, which records a correlation coefficient of 0.98 (Figs. 8c,d). Now, as CP events are typically meridionally broader than EP events, as has been shown above for the peak-ENSO event period (Figs. 3b, 4c,f,i and 5b), they have a larger influence on winds in the off-equatorial region and the zonal winds along 5°N and 5°S (Figs. 4c,f,i) that determine the Ekman transport into the WWV region. This relationship appears to be enhanced during the pre-ENSO event period where off-equatorial wind stresses are most solely a function CP events ($r = 0.95$), while EP events have a negligible role ($r = -0.14$) (not shown). The prominent role of CP events is also clear in Fig. 8, where CP event magnitude appears to play a strong role modulating pre-ENSO event WWV (Figs. 8a,c, when EP event magnitude is fixed), while EP event magnitude plays a negligible role (Figs. 8b,d, when CP event magnitude is fixed).

To understand what is driving the pre-ENSO event WWVs, we calculate (offline) the estimated WWV changes in this pre-event period due to Ekman and meridional geostrophic transports along 5°N and 5°S (not shown). First, we find a strong positive correlation ($r = 0.92$) between the Ekman-induced pre-event WWV changes and those WWV changes modeled (Fig. 7, center), while we also find a reasonably strong negative correlation ($r = -0.78$) between the geostrophic WWV changes and those WWV changes shown in Fig. 7 (center panel). The WWVs estimated by combining Ekman and geostrophic WWV changes (not shown) compare very well to that directly output from the model (Fig. 7, center panel), with a correlation coefficient of 0.97. In regard to what is driving CP induced pre-event WWVs, the results of this analysis highlight a strong positive relationship between CP events and the pre-event WWVs generated due to Ekman transport calculated along 5°N and 5°S ($r = 0.90$; $b = 4.67 \times 10^{13}$ m^{-3}), and a strong, but weaker, negative relationship between CP events and the pre-event WWVs generated due to meridional geostrophic transport ($r = -0.74$; $b = -1.88 \times 10^{13}$ m^{-3}). As the CP events generate an Ekman transport into the WWV region whose magnitude is approximately 2.5 times larger than the opposing geostrophically induced WWV changes they induce, the resulting WWV changes are predominately driven by Ekman transport.

As to why EP events do not appear to modulate pre-ENSO event WWV, our results highlight a moderate positive relationship between EP events with the Ekman transport calculated along 5°N and 5°S ($r = 0.42$; $b = 2.18 \times 10^{13}$ m^{-3}), and a similar strength and magnitude negative relationship between EP events with the meridional geostrophic transport calculated along 5°N and 5°S ($r = -0.65$; $b = -1.66 \times 10^{13}$ m^{-3}). Thus, EP events appear to generate pre-event Ekman transports into the WWV region, but they also generate opposing meridional geostrophic transports into the WWV that are of the opposite sign and of similar magnitude. Thus, due to cancelation between Ekman and geostrophic transports into the WWV region, EP events result in very little actual pre-event WWV change. This signal cancelation during EP events is also seen as east–west contrasts of pre-event WWVs, where the western and eastern Pacific WWV responses largely cancel out in the basin wide average (cf. Fig. 7, panel EP:0, CP:1 with panel EP:1 and CP:0), suggestive of a strong east–west tilt of the thermocline during EP events in this pre-ENSO event period.

b. EP/CP post-ENSO event WWV differences

As discussed above, post-ENSO event WWV changes are often thought of as triggers for the termination of the events (Jin 1997; Meinen and McPhaden 2000; Burgers et al. 2005). In these experiments we analyze the post-ENSO event average WWV during the March–May period following the events December peak (Fig. 7, pink region of outer panels). Similar results can be found if we instead analyze the western Pacific WWV during the event peak, which is consistent with the results of Planton et al. (2018) and Neske et al. (2021). Plotting post-ENSO event WWV against the peak equatorial wind stress (Figs. 9a,b), reveals relatively strong relationship between the two, with a correlation coefficient of −0.80. A similar result is found plotting the post-ENSO event WWV

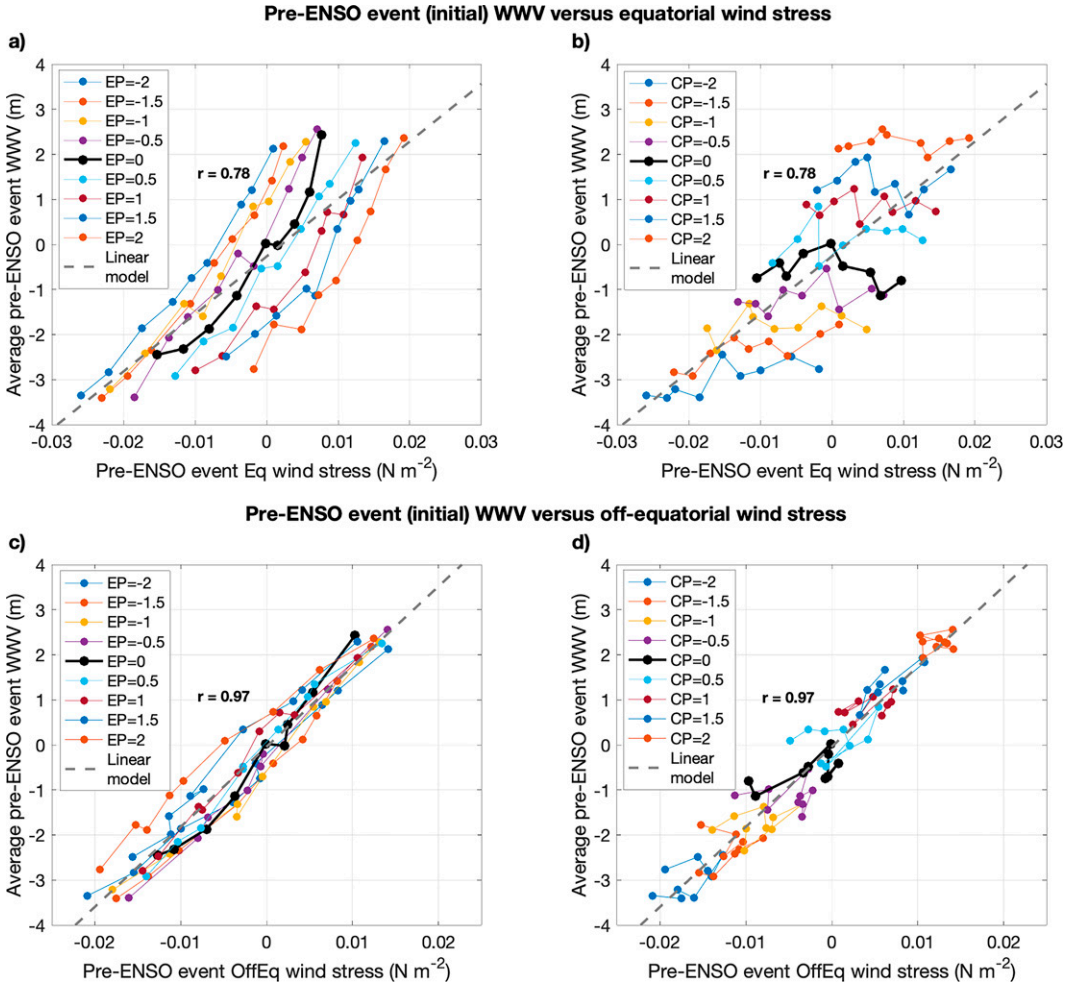

FIG. 8. Average pre-ENSO event WWV (defined as the July–September average WWV before the ENSO event peak) plotted against (a),(b) equatorial zonal wind stress and (c),(d) off-equatorial wind stress. Note, (a) and (b) display the same data, the difference is whether the plotted colors are chosen to highlight EP events (when CP events of fixed magnitude are displayed, see legend) or CP events (when EP events of fixed magnitude are displayed, see legend). The above statement also directly relates to the data presented in (c) and (d).

against the peak Niño-3.4 region SSTA (not shown, $r = -0.87$). However, there is clearly a lot of scatter, which suggests that equatorial zonal wind stress or Niño-3.4 SSTA alone are not the sole drivers of post-ENSO event WWV.

Looking at the magnitude of predicted postevent WWV (Fig. 10b), where the postevent WWVs are predicted using the linear regression model with equatorial region wind stresses depicted by the dashed black line in Figs. 9a and 9b, reveals significant differences with the modeled postevent WWV (Figs. 10a,c). The largest differences are negative in the bottom right corner (i.e., for positive EP events and negative CP events) and positive in the top left corner (i.e., for negative EP events and positive CP events) (Fig. 10c), in what can be perceived as a clockwise rotation of the actual postevent WWV changes compared to those predicted with equatorial wind stresses. Furthermore, the postevent WWV appears to be more a function of EP event magnitude ($r = -0.89$) than CP event magnitude ($r = -0.41$) (Fig. 10a), while the opposite is true for equatorial wind stresses and postevent WWV predicted with the same stresses (Fig. 10b). The large differences seen between actual (Fig. 10a) and equatorial wind stress predicted postevent WWV (Fig. 10b) suggest that post-ENSO event WWV cannot accurately be predicted with only knowledge of equatorial zonal wind stress anomalies (Fig. 10c).

Plotting the postevent WWV against the near-equatorial wind stress curl (Figs. 9c,d) reveals a much stronger correlation ($r = -0.97$), and much less scatter is seen as compared to when plotting the postevent WWV against equatorial wind stress ($r = -0.8$ Figs. 9a,b). As discussed above in section 3a, the focus on wind stress curl here is because it is known to drive thermocline depth changes off the equator, while geostrophic transports created due near-equatorial thermocline depth changes can drive WWV changes. A somewhat similar

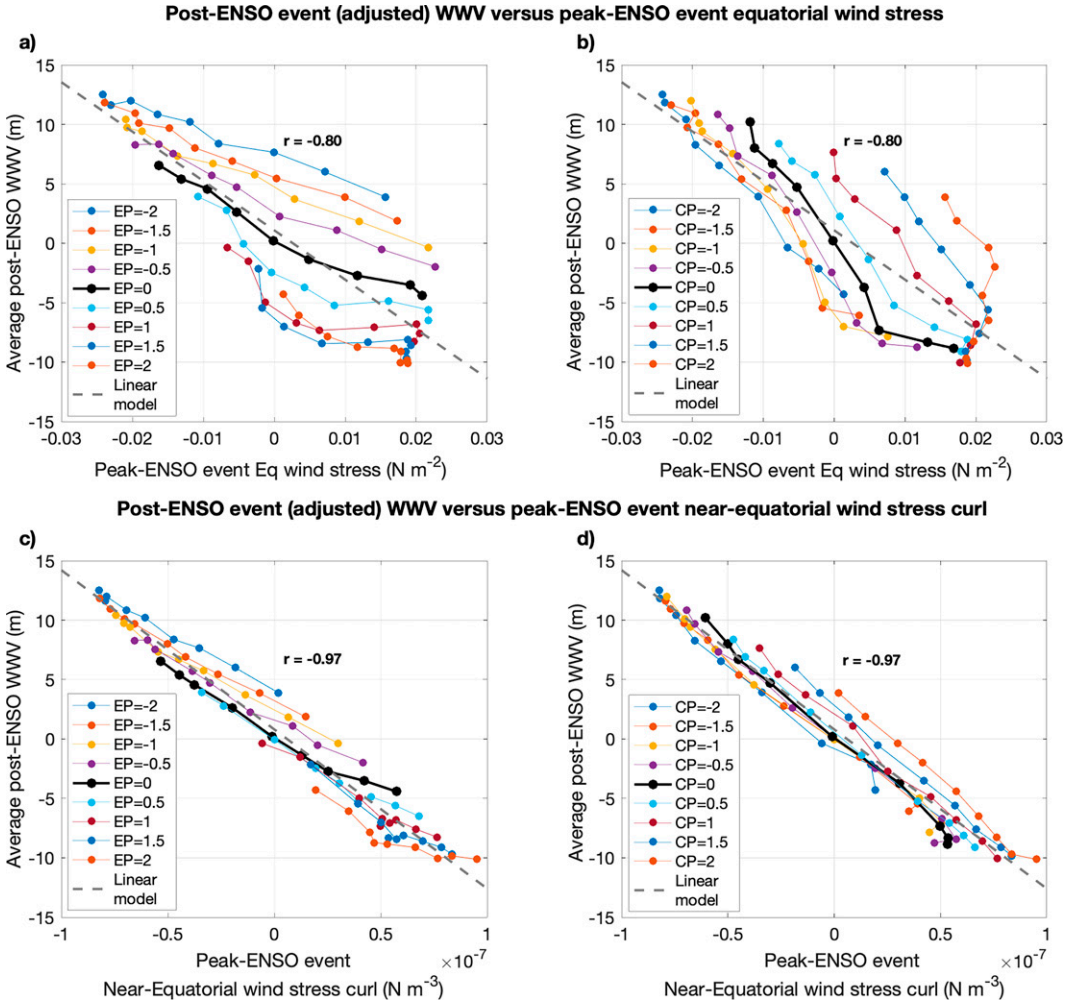

FIG. 9. Average post-ENSO event WWV (defined as the March–May average WWV after the ENSO event peak) plotted against the (a),(b) ENSO event peak equatorial wind stress and (c),(d) wind stress curl. Note, (a) and (b) display the same data, the difference is whether the plotted colors are chosen to highlight EP events (when CP events of fixed magnitude are displayed) or CP events (when EP events of fixed magnitude are displayed). The above statement also directly relates to the data presented in (c) and (d).

result is also found in the observations, where post-ENSO event WWV displays a stronger relationship with peak-ENSO event near-equatorial wind stress curl ($r = -0.68$) than it displays with peak-ENSO event equatorial zonal wind stress ($r = -0.53$; Fig. 11). It is also noted that (i) any identified relationship in our idealized experiments (whether it be with equatorial zonal wind stress or near-equatorial wind stress curl) is likely enhanced by the lack of atmospheric noise throughout the majority of this post-ENSO event period, as the applied wind stress forcing is set to zero in April after the event peak; and (ii) the same idealized conditions do not apply in the observations. Figures 9b and 9d (when CP event magnitude is fixed) also show that EP event magnitude plays a strong role modulating postevent WWV, while CP event magnitude plays a much smaller role (Figs. 9a,c, when EP event magnitude is fixed). Correlations between postevent WWV and EP event magnitude support this visual analysis ($r = -0.89$) and suggest that EP event magnitude alone can explain ~80% of the WWV variance, which is much larger than the ~17% of WWV variance that can be explained with CP event magnitude ($r = -0.41$) (Fig. 10a). This is somewhat expected as the results presented in section 3a suggested that zonal wind stress curl is largely a function of EP events only ($r = 0.80$). Thus, the post-ENSO event WWV, during both El Niño and La Niña phases, is much better modeled as function of near-equatorial zonal wind stress curl than as a function of equatorial zonal wind stress. It is also notable that virtually no asymmetry exists between ENSO phases. This result somewhat expected given the underlying role of ocean dynamics in the post-ENSO event WWV response, and the prominent role wind stress curl plays in driving the adjusted ocean dynamic response.

The importance of the structure of the wind response is highlighted by the fact that for very similar equatorial zonal

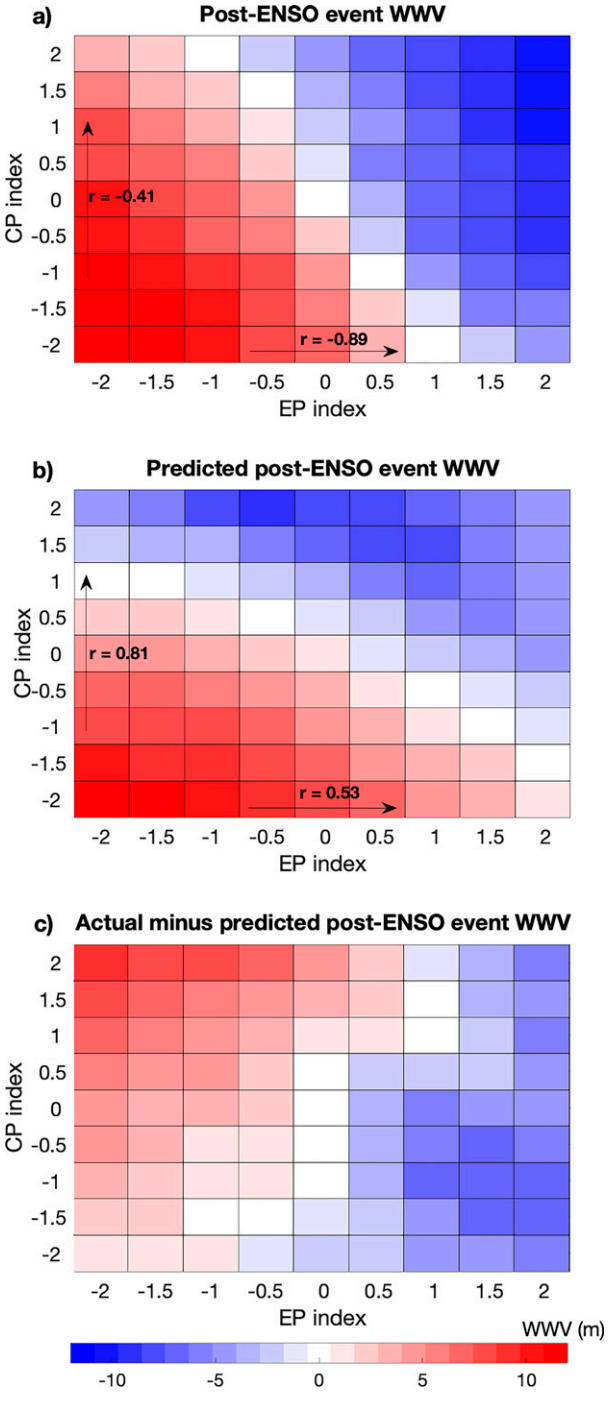

FIG. 10. (a) The average post-ENSO event WWV (defined as the average WWV 4–6 months after the event peak) is shown, and (b) the post-ENSO event WWV predicted from equatorial wind stress using the relationship depicted in Fig. 8a (dashed gray line). (c) The difference between (a) and (b) is displayed.

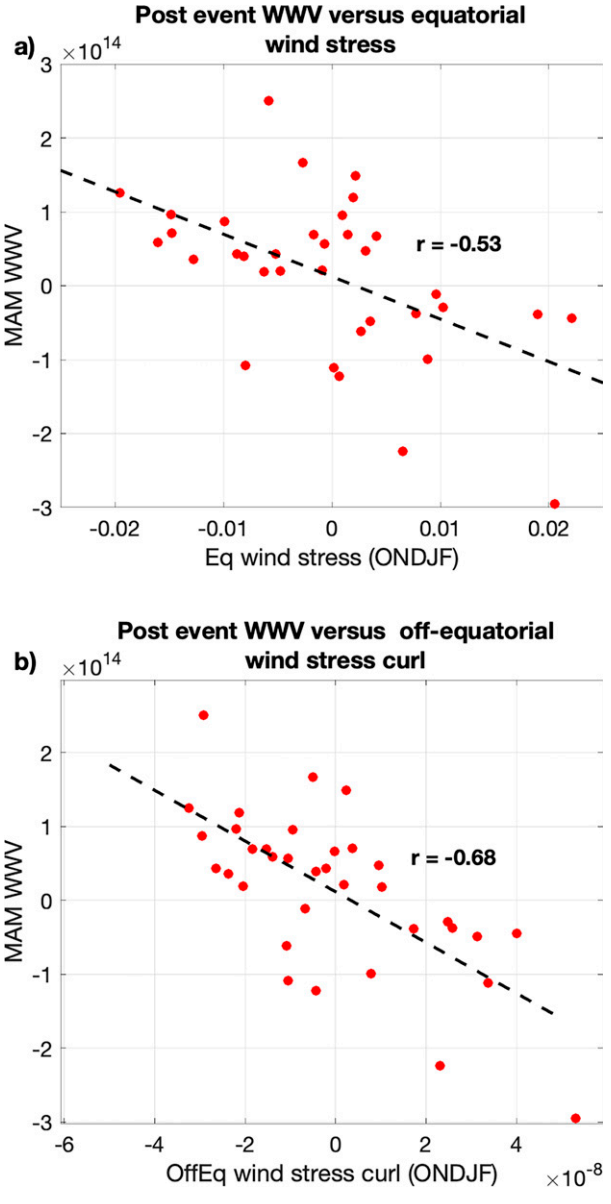

FIG. 11. Observed average post-ENSO event WWV (defined as the March–May average WWV after the ENSO event peak) plotted against peak-ENSO event (October–February) (a) equatorial zonal wind stress and (b) near-equatorial zonal wind stress curl.

wind magnitudes, you can have very different WWV responses (Figs. 9a,b). Furthermore, when separating the equatorial zonal wind stresses according to their sign (i.e., where positive wind stress anomalies are typically associated with El Niño–like warming and negative wind stress anomalies are typically associated with La Niña–like cooling), the correlation coefficient for positive equatorial wind stress values and postevent WWVs is much closer to zero at −0.36, than the same relationship for negative equatorial wind stress values ($r = -0.82$) (Figs. 9a,b). As such, a large negative equatorial wind stress, like those that occur during a La Niña event peak, will typically lead to a large post-ENSO event WWV recharge. On the other hand, a large positive equatorial wind stress during an El Niño event, will not always result in a large discharge in the post-ENSO event WWV and a small post-

ENSO event increase in WWV is also possible (Figs. 8a,b). This implies that, given the same diversity in SSTAs, positive zonal equatorial wind stress (El Niño) events have a larger diversity in their spatial structure than negative equatorial wind stress (La Niña) events.

5. Discussion and conclusions

In this manuscript we investigated observations, along with carrying out a series of numerical experiments to thoroughly explore the role SSTA structure and location (i.e., EP- and CP-type ENSO events) play modulating the meridional extent of the surface wind response. We also carried out a series on linear Shallow Water Model (SWM) simulations to better understand the impact of these wind response differences have on the pre and post-ENSO event WWV. The WWV focus is because previous literature suggests that pre-ENSO event WWV changes are important precursors of ENSO events, while post-ENSO event WWV changes are often associated with the termination of ENSO events (Jin 1997; Meinen and McPhaden 2000; Burgers et al. 2005). It is important to note that while utilizing uncoupled AGCM and simple ocean models experiments separately allows us to simplify a complex problem and allows for a clear comparison of the impact of ENSO SSTA diversity, it also removes the ocean–atmosphere coupling that is fundamental to ENSO. Thus, the results of this work act as an initial guide as to how ENSO SSTA diversity make impact ENSOs dynamics, further experimentation with more complex models and experiments will likely be required to refine details of the relationships identified here.

Our AGCM experiments and observational analysis suggest that both EP and CP events, which both project onto Niño-3.4 region SSTA, modulate equatorial zonal wind stresses (5°N–5°S). Although, our results also suggest that CP events appear to play a slightly stronger role in the modulation of equatorial zonal wind stresses. On the other hand, both lines of evidence show that EP and CP events have distinctly different off-equatorial wind stress responses. That is, CP events are positively correlated with off-equatorial zonal wind stresses (5°–10° latitude), while EP events have either a negative correlation (AGCM experiments) or near-zero correlation (observations). Both of these results, which are broadly consistent with the work of Neske et al. (2021), show that EP and CP events have distinctly different off-equatorial wind stress responses such that CP-type events generate a zonal wind stress response that is typically meridionally broader than EP events. Initial results from an additional series of AGCM experiments suggest that these changes in zonal wind stress meridional extent in CP events are at least partially due to the increased meridional extent of the underlying SSTA.

Changes in the meridional structure of equatorial zonal wind have been considered important for the period of ENSO (e.g., Kirtman 1997; Capotondi et al. 2006), but meridional structure differences between ENSO event flavors have not been identified prior to this study. We note that several studies have focused on the EP and CP event differences in the zonal extent and longitude of the anomalous zonal wind stress maximum, where CP events generally display zonal stresses that are displaced to the west of those during EP events (e.g., Kug et al. 2009). The similarity between the average equatorial zonal wind stress response for EP and CP events implies that it would be very difficult to distinguish between event types if provided with the magnitude of equatorial wind stress alone. This is important as it suggests that current conceptual models of ENSO, which have ocean feedbacks based solely on equatorial zonal wind stress akin to having a fixed wind stress pattern, would not be able to represent the diversity of this atmospheric response. Further to this, while the representation of ENSO diversity is improving in CMIP class models, it is usually assessed in terms of the location of maximum warming (e.g., Chen et al. 2017). As such, it is currently unclear whether these models can reproduce the increased meridional extend of CP event SSTAs.

This zonal wind stress pattern difference between CP and EP events is most prominently highlighted in the near-equatorial wind stress curl (2°–8° latitude). As EP events typically transition from a strong equatorial zonal wind stress response to a weak (observations) or opposite signed (AGCM experiments) off-equatorial wind response, they typically display a strong relationship with near-equatorial zonal wind stress curl. On the other hand, the typically meridionally broad CP event zonal wind stress response is consistent with a weaker relationship with near-equatorial wind stress curl. In fact, coefficient of determination (r^2) suggests that EP events explain more than double the near-equatorial zonal wind stress curl variance of CP events, a result that is consistent in both, our idealized AGCM experiments and the observed wind response. Given that the post-ENSO event adjusted ocean response is a function of wind stress curl through the initiation of oceanic Rossby waves, these strong EP and CP event near-equatorial curl differences suggest that these off-equatorial wind stress changes have the potential to significantly impact the temporal evolution of ENSO events. Im et al. (2015) reported an asymmetry in the meridional width of the zonal wind response between El Niño (narrow) and La Niña (wide) events, while also showing that these width differences led to a larger sensitivity of the oceanic response to wind stress forcing in El Niño events compared to La Niña events.

A build up (discharge) of WWV is often considered a precursor of El Niño (La Niña) events (Meinen and McPhaden 2000). The work of Neske and McGregor (2018), qualitatively agreed with the study of Kessler (2002), showing that roughly half of these initial changes in WWV are an instantaneous response to anomalous wind stress forcing, rather than slow ocean dynamics response suggested by ENSO conceptual models. Here our results show that while equatorial wind stresses can provide a reasonable estimate of pre-ENSO event WWV ($r = 0.78$, $r^2 = 0.61$), off-equatorial wind stresses provide a much more accurate estimate ($r = 0.97$, $r^2 = 0.94$). Further to this, what is also clear from our analysis is that CP event magnitude is almost solely responsible modulating initial WWV ($r = 0.98$), while EP event magnitude plays a

negligible role in modulating initial WWV ($r = -0.11$). Our analysis suggests that these pre-event WWV changes are largely due to Ekman transport along 5°N and 5°S into the equatorial region, though we do identify a compensating geostrophic transport that is important for minimizing the pre-event WWVs of EP events. It is noted that the idealized experiment set up utilized here only focused on understanding the role of wind stresses in modulating pre-ENSO event WWV (i.e., the ocean dynamic response from preceding ENSO events had been neglected). We would expect the dominance of the CP events to remain on total wind driven component of pre-ENSO event WWV change in a different experiment format. However, as the wind driven WWV changes are one of two components that can drive pre-ENSO event WWV in the observations, we expect the role CP events to be reduced in the changes observed.

Conceptual models of ENSO suggest a discharge (build up) of WWV is often considered to lead to the termination of El Niño (La Niña) events (Jin 1997). This change in WWV is thought to be predominantly underpinned by the slow ocean dynamical processes described by Sverdrup transport (Jin 1997). Other components are also known to play a role in the discharge of WWV during El Niño events are the meridional movement of ENSO anomalous winds (McGregor et al. 2012, 2013a; Abellán and McGregor 2016), which are generated by interaction between ENSO and the seasonal cycle (Stuecker et al. 2013, 2015, 2016), and western Pacific wind changes driven by interbasin interactions (Okumura et al. 2011). However, these are not the focus of the present study.

ENSO conceptual models typically assume that the discharge (recharge) of WWV during an El Niño (La Niña) event is a function of the equatorial wind stress (Jin 1997; Burgers et al. 2005; Clarke et al. 2007). As discussed above, this simplification is akin to making an assumption that the anomalous winds accompanying all ENSO events can be represented by a single pattern. Similar assumptions were initially made about SSTA patterns of ENSO events; however, since the early 2000s the community has attempted to more systematically classify ENSO event diversity (Capotondi et al. 2015, 2020). Our results suggest that a similar transition needs to occur for surface wind stresses as it is becoming apparent that while the explicit representation of the wind stress curl may not be essential for conceptual models of ENSO to operate (Clarke et al. 2007; Zhu et al. 2017), it is proposed to play a prominent role in both, the pre to post-2000 changes in the WWV–ENSO SSTA relationship (Neske et al. 2021), and ENSO phase asymmetries (Im et al. 2015). These results are supported by the experiments carried out here that show correlations between wind stress curl and post-ENSO event WWV have a much stronger correlation ($r = -0.97$, $r^2 = 0.94$) than that of equatorial wind stress alone ($r = -0.8$, $r^2 = 0.64$). Further to this, the positive correlation between EP event magnitude and equatorial wind stress along with the negative correlation between EP event magnitude and off-equatorial wind stress ensures that EP event magnitude plays a prominent role in modulating our estimated wind stress curl. As a result, we also find a stronger relationship between EP event magnitude and the postevent WWV ($r = -0.89$) compared to the relationship between CP event magnitude and postevent WWV ($r = -0.41$). This latter finding suggests that EP- and CP-type ENSO events may have a distinctly different balance of feedbacks underpinning their termination, as CP events are less reliant on the traditional discharge of WWV. This result is broadly consistent with several earlier studies that identified weaker WWV changes occurring during CP events when compared to EP events (Kug et al. 2009, 2010; Singh and Delcroix 2013).

Thus, whether you are interested in distinguishing EP and CP events, or modeling the pre and post ENSO event WWVs, or understanding the predictability of ENSO event phase transitions, the results presented here suggest the inclusion of wind stresses in the off-equatorial region and near-equatorial wind stress curl is essential. Furthermore, our results suggest that simply adding additional SSTA diversity to conceptual models of ENSO is not enough, these models require explicit representation of off-equatorial zonal wind stresses and near-equatorial wind stress curl to represent ENSO diversity in the underlying dynamics. This does not mean that our conceptual models are incorrect, as all of the processes represented in these models still appear to operate. However, it seems that the balance of processes determining the growth and termination of the event likely varies with event type (CP or EP). For instance, in the framework of the ENSO recharge oscillator model, our results suggest that EP events have stronger coupling between sea surface temperatures (SST) and thermocline (WWV), supporting more clearly the oscillating nature of EP events than CP events. This would also imply a more predictable element in the EP event termination and phase transition. In turn, the growth rate of SST is related to the wind-driven pre-event WWV changes that are stronger in CP events. Although we identify further important dynamical differences between EP- and CP-type ENSO events, the main results of this work agree with the earlier work of Ren and Jin (2013), who suggest that the current conceptual models may need to operate with different sets of parameters depending on the event type they are trying to represent.

Acknowledgments. This work was supported by the Australian Research Council (ARC) including FT160100162, DP200102329, and CE170100023. Finally, we thank J.-S. Kug and two anonymous reviewers for their very valuable feedback that helped improve this manuscript.

REFERENCES

Abellán, E., and S. McGregor, 2016: The role of the southward wind shift in both, the seasonal synchronization and duration of ENSO events. *Climate Dyn.*, **47**, 509–527, https://doi.org/10.1007/s00382-015-2853-1.

Bi, D., and Coauthors, 2013: The ACCESS coupled model: Description, control climate and evaluation. *Aust. Meteor. Oceanogr. J.*, **63**, 41–64, https://doi.org/10.22499/2.6301.004.

Bunge, L., and A. J. Clarke, 2014: On the warm water volume and its changing relationship with ENSO. *J. Phys. Oceanogr.*, **44**, 1372–1385, https://doi.org/10.1175/JPO-D-13-062.1.

Burgers, G., F. F. Jin, and G. J. van Oldenborgh, 2005: The simplest ENSO recharge oscillator. *Geophys. Res. Lett.*, **32**, L13706, https://doi.org/10.1029/2005GL022951.

Capotondi, A., A. Wittenberg, and S. Masina, 2006: Spatial and temporal structure of tropical Pacific interannual variability in 20th century coupled simulations. *Ocean Modell.*, **15**, 274–298, https://doi.org/10.1016/j.ocemod.2006.02.004.

——, and Coauthors, 2015: Understanding ENSO diversity. *Bull. Amer. Meteor. Soc.*, **96**, 921–938, https://doi.org/10.1175/BAMS-D-13-00117.1.

——, C. Deser, A. S. Phillips, Y. Okumura, and S. M. Larson, 2020: ENSO and Pacific decadal variability in the community Earth System Model version 2. *J. Adv. Model. Earth Syst.*, **12**, e2019MS002022, https://doi.org/10.1029/2019MS002022.

Chen, C., M. A. Cane, A. T. Wittenberg, and D. Chen, 2017: ENSO in the CMIP5 simulations: Life cycles, diversity, and responses to climate change. *J. Climate*, **30**, 775–801, https://doi.org/10.1175/JCLI-D-15-0901.1.

Clarke, A. J., 2008: *An Introduction to the Dynamics of El Niño and the Southern Oscillation*. Academic Press, 324 pp.

——, S. Van Gorder, and G. Colantuono, 2007: Wind stress curl and ENSO discharge/recharge in the equatorial Pacific. *J. Phys. Oceanogr.*, **37**, 1077–1091, https://doi.org/10.1175/JPO3035.1.

Davies, T., M. J. P. Cullen, A. J. Malcolm, M. H. Mawson, A. Staniforth, A. A. White, and N. Wood, 2005: A new dynamical core for the Met Office's global and regional modelling of the atmosphere. *Quart. J. Roy. Meteor. Soc.*, **131**, 1759–1782, https://doi.org/10.1256/qj.04.101.

Dee, D. P., and S. Uppala, 2009: Variational bias correction of satellite radiance data in the ERA-Interim reanalysis. *Quart. J. Roy. Meteor. Soc.*, **135**, 1830–1841, https://doi.org/10.1002/qj.493.

Diaz, H. F., M. P. Hoerling, and J. K. Eischeid, 2002: ENSO variability, teleconnections and climate change. *Int. J. Climatol.*, **21**, 1845–1862, https://doi.org/10.1002/joc.631.

DiNezio, P. N., and C. Deser, 2014: Nonlinear controls on the persistence of La Niña. *J. Climate*, **27**, 7335–7355, https://doi.org/10.1175/JCLI-D-14-00033.1.

Dommenget, D., T. Bayr, and C. Frauen, 2013: Analysis of the non-linearity in the pattern and time evolution of El Niño–Southern Oscillation. *Climate Dyn.*, **40**, 2825–2847, https://doi.org/10.1007/s00382-012-1475-0.

Fu, X., and B. Wang, 1999: The role of longwave radiation and boundary layer thermodynamics in forcing tropical surface winds. *J. Climate*, **12**, 1049–1069, https://doi.org/10.1175/1520-0442(1999)012<1049:TROLRA>2.0.CO;2.

Frauen, C., and D. Dommenget, 2010: El Niño and La Niña amplitude asymmetry caused by atmospheric feedbacks. *Geophys. Res. Lett.*, **37**, L18801, https://doi.org/10.1029/2010GL044444.

——, ——, N. Tyrrell, M. Rezny, and S. Wales, 2014: Analysis of the nonlinearity of El Niño–Southern Oscillation teleconnections. *J. Climate*, **27**, 6225–6244, https://doi.org/10.1175/JCLI-D-13-00757.1.

Gill, A. E., 1980: Some simple solutions for heat induced tropical circulation. *Quart. J. Roy. Meteor. Soc.*, **106**, 447–462, https://doi.org/10.1002/qj.49710644905.

Goddard, L., and A. Gershunov, 2020: Impact of El Niño on weather and climate extremes. *El Niño Southern Oscillation in a Changing Climate*, M. J. McPhaden, A. Santoso, and W. Cai, Eds., Amer. Geophys. Union, 361–375, https://doi.org/10.1002/9781119548164.ch16.

Im, S.-H., S.-I. An, S. T. Kim, and F.-F. Jin, 2015: Feedback processes responsible for El Niño–La Niña amplitude asymmetry. *Geophys. Res. Lett.*, **42**, 5556–5563, https://doi.org/10.1002/2015GL064853.

Izumo, T., M. Lengaigne, J. Vialard, I. Suresh, and Y. Planton, 2019: On the physical interpretation of the lead relation between warm water volume and the El Niño–Southern Oscillation. *Climate Dyn.*, **52**, 2923–2942, https://doi.org/10.1007/s00382-018-4313-1.

Jin, F.-F., 1997: An equatorial ocean recharge paradigm for ENSO. Part I: Conceptual model. *J. Atmos. Sci.*, **54**, 811–829, https://doi.org/10.1175/1520-0469(1997)054<0811:AEORPF>2.0.CO;2.

Kao, H. Y., and J. Y. Yu, 2009: Contrasting Eastern-Pacific and Central-Pacific types of ENSO. *J. Climate*, **22**, 615–632, https://doi.org/10.1175/2008JCLI2309.1.

Kessler, W. S., 2002: Is ENSO a cycle or a series of events? *Geophys. Res. Lett.*, **29**, 2125, https://doi.org/10.1029/2002GL015924.

Kirtman, B. P., 1997: Oceanic Rossby wave dynamics and the ENSO period in a coupled model. *J. Climate*, **10**, 1690–1704, https://doi.org/10.1175/1520-0442(1997)010<1690:ORWDAT>2.0.CO;2.

Kug, J. S., F. F. Jin, and S. Il An, 2009: Two types of El Niño events: Cold tongue El Niño and warm pool El Niño. *J. Climate*, **22**, 1499–1515, https://doi.org/10.1175/2008JCLI2624.1.

——, J. Choi, S. Il An, and F. F. Jin, 2010: Warm pool and cold tongue El Niño events as simulated by the GFDL 2.1 coupled GCM. *J. Climate*, **23**, 1226–1239, https://doi.org/10.1175/2009JCLI3293.1.

Lindzen, R. S., and S. Nigam, 1987: On the role of sea surface temperature gradients in forcing low-level winds and convergence in the tropics. *J. Atmos. Sci.*, **44**, 2418–2436, https://doi.org/10.1175/1520-0469(1987)044<2418:OTROSS>2.0.CO;2.

Martin, G. M., S. F. Milton, C. A. Senior, M. E. Brooks, S. Ineson, T. Reichler, and J. Kim, 2010: Analysis and reduction of systematic errors through a seamless approach to modeling weather and climate. *J. Climate*, **23**, 5933–5957, https://doi.org/10.1175/2010JCLI3541.1.

——, and Coauthors, 2011: The HadGEM2 family of Met Office Unified Model climate configurations. *Geosci. Model Dev.*, **4**, 723–757, https://doi.org/10.5194/gmd-4-723-2011.

McGregor, S., N. J. Holbrook, and S. B. Power, 2007: Interdecadal sea surface temperature variability in the equatorial Pacific Ocean. Part I: The role of off-equatorial wind stresses and oceanic Rossby waves. *J. Climate*, **20**, 2643–2658, https://doi.org/10.1175/JCLI4145.1.

——, A. Timmermann, N. Schneider, M. F. Stuecker, and M. H. England, 2012: The effect of the South Pacific convergence zone on the termination of El Niño events and the meridional asymmetry of ENSO. *J. Climate*, **25**, 5566–5586, https://doi.org/10.1175/JCLI-D-11-00332.1.

——, N. Ramesh, P. Spence, M. H. England, M. J. McPhaden, and A. Santoso, 2013a: Meridional movement of wind anomalies during ENSO events and their role in event termination. *Geophys. Res. Lett.*, **40**, 749–754, https://doi.org/10.1002/grl.50136.

——, A. Timmermann, M. H. England, O. Elison Timm, and A. T. Wittenberg, 2013b: Inferred changes in El Niño–Southern Oscillation variance over the past six centuries. *Climate Past*, **9**, 2269–2284, https://doi.org/10.5194/cp-9-2269-2013.

McPhaden, M. J., 2012: A 21st century shift in the relationship between ENSO SST and warm water volume anomalies. *Geophys. Res. Lett.*, **39**, L09706, https://doi.org/10.1029/2012GL051826.

——, S. E. Zebiak, and M. H. Glantz, 2006: ENSO as an integrating concept in earth science. *Science*, **314**, 1740–1745, https://doi.org/10.1126/science.1132588.

——, T. Lee, and D. McClurg, 2011: El Niño and its relationship to changing background conditions in the tropical Pacific Ocean. *Geophys. Res. Lett.*, **38**, L15709, https://doi.org/10.1029/2011GL048275.

Meinen, C. S., and M. J. McPhaden, 2000: Observations of warm water volume changes in the equatorial Pacific and their relationship to El Niño and La Niña. *J. Climate*, **13**, 3551–3559, https://doi.org/10.1175/1520-0442(2000)013<3551:OOWWVC>2.0.CO;2.

——, and ——, 2001: Interannual variability in warm water volume transports in the equatorial Pacific during 1993–99. *J. Phys. Oceanogr.*, **31**, 1324–1345, https://doi.org/10.1175/1520-0485(2001)031<1324:IVIWWV>2.0.CO;2.

Neske, S., and S. McGregor, 2018: Understanding the warm water volume precursor of ENSO events and its interdecadal variation. *Geophys. Res. Lett.*, **45**, 1577–1585, https://doi.org/10.1002/2017GL076439.

——, ——, M. Zeller, and D. Dommenget, 2021: Wind spatial structure triggers ENSO's oceanic warm water volume changes. *J. Climate*, **34**, 1985–1999, https://doi.org/10.1175/JCLI-D-20-0040.1.

Okumura, Y. M., M. Ohba, C. Deser, and H. Ueda, 2011: A proposed mechanism for the asymmetric duration of El Niño and La Niña. *J. Climate*, **24**, 3822–3829, https://doi.org/10.1175/2011JCLI3999.1.

Picaut, J., F. Masia, and Y. du Penhoat, 1997: An advective-reflective conceptual model for the oscillatory nature of the ENSO. *Science*, **277**, 663–666, https://doi.org/10.1126/science.277.5326.663.

Planton, Y., J. Vialard, E. Guilyardi, M. Lengaigne, and T. Izumo, 2018: Western Pacific Oceanic heat content: A better predictor of La Niña than of El Niño. *Geophys. Res. Lett.*, **45**, 9824–9833, https://doi.org/10.1029/2018GL079341.

Qiu, B., and S. Chen, 2010: Interannual-to-decadal variability in the bifurcation of the north equatorial current off the Philippines. *J. Phys. Oceanogr.*, **40**, 2525–2538, https://doi.org/10.1175/2010JPO4462.1.

Rayner, N. A., D. E. Parker, E. B. Horton, C. K. Folland, L. V. Alexander, and D. P. Rowell, 2003: Global analyses of sea surface temperature, sea ice, and night marine air temperature since the late nineteenth century. *J. Geophys. Res.*, **108**, 4407, https://doi.org/10.1029/2002JD002670.

Ren, H.-L., and F.-F. Jin, 2013: Recharge oscillator mechanisms in two types of ENSO. *J. Climate*, **26**, 6506–6523, https://doi.org/10.1175/JCLI-D-12-00601.1.

Santoso, A., and Coauthors, 2019: Dynamics and predictability of El Niño–Southern oscillation: An Australian perspective on progress and challenges. *Bull. Amer. Meteor. Soc.*, **100**, 403–420, https://doi.org/10.1175/BAMS-D-18-0057.1.

Singh, A., and T. Delcroix, 2013: Eastern and Central Pacific ENSO and their relationships to the recharge/discharge oscillator paradigm. *Deep-Sea Res. I*, **82**, 32–43, https://doi.org/10.1016/j.dsr.2013.08.002.

Smith, N. R., 1995: The BMRC ocean thermal analysis system. *Aust. Meteor. Mag.*, **44**, 93–110.

Sprintall, J., S. Cravatte, B. Dewitte, Y. Du, and A. Sen Gupta, 2020: ENSO oceanic teleconnections. *El Niño Southern Oscillation in a Changing Climate*, M. J. McPhaden, A. Santoso, and W. Cai, Eds., Amer. Geophys. Union, 337–359, https://doi.org/10.1002/9781119548164.ch15.

Stuecker, M. F., A. Timmermann, F.-F. Jin, S. McGregor, and H.-L. Ren, 2013: A combination mode of the annual cycle and the El Niño/southern oscillation. *Nat. Geosci.*, **6**, 540–544, https://doi.org/10.1038/ngeo1826.

——, F.-F. Jin, A. Timmermann, and S. McGregor, 2015: Combination mode dynamics of the anomalous northwest Pacific anticyclone. *J. Climate*, **28**, 1093–1111, https://doi.org/10.1175/JCLI-D-14-00225.1.

——, ——, ——, and ——, 2016: Reply to "Comments on 'Combination mode dynamics of the anomalous northwest Pacific anticyclone.'" *J. Climate*, **29**, 4695–4706, https://doi.org/10.1175/JCLI-D-15-0558.1.

Suarez, M. J., and P. S. Schopf, 1988: A delayed action oscillator for ENSO. *J. Atmos. Sci.*, **45**, 3283–3287, https://doi.org/10.1175/1520-0469(1988)045<3283:ADAOFE>2.0.CO;2.

Takahashi, K., A. Montecinos, K. Goubanova, and B. Dewitte, 2011: ENSO regimes: Reinterpreting the canonical and Modoki El Niño. *Geophys. Res. Lett.*, **38**, L10704, https://doi.org/10.1029/2011GL047364.

Taschetto, A. S., R. R. Rodrigues, G. A. Meehl, S. McGregor, and M. H. England, 2016a: How sensitive are the Pacific–tropical North Atlantic teleconnections to the position and intensity of El Niño-related warming? *Climate Dyn.*, **46**, 1841–1860, https://doi.org/10.1007/s00382-015-2679-x.

——, ——, ——, ——, and ——, 2016b: How sensitive are the Pacific–tropical North Atlantic teleconnections to the position and intensity of El Niño-related warming? *Climate Dyn.*, **46**, 1841–1860, https://doi.org/10.1007/s00382-015-2679-x.

——, C. C. Ummenhofer, M. F. Stuecker, D. Dommenget, K. Ashok, R. R. Rodrigues, and S.-W. Yeh, 2020: ENSO atmospheric teleconnections. *El Niño Southern Oscillation in a Changing Climate*, M. J. McPhaden, A. Santoso, and W. Cai, Eds., Amer. Geophys. Union, 309–335, https://doi.org/10.1002/9781119548164.ch14.

Timmermann, A., and Coauthors, 2019: Author correction: El Niño–Southern Oscillation complexity. *Nature*, **567**, E3, https://doi.org/10.1038/s41586-019-0994-9.

Wang, C., and J. Picaut, 2004: *Understanding ENSO Physics—A Review. Geophys. Monogr.*, Vol. 147, Amer. Geophys. Union, 21–48.

Weisberg, R. H., and C. Wang, 1997: A Western Pacific oscillator paradigm for the El Niño–Southern Oscillation. *Geophys. Res. Lett.*, **24**, 779–782, https://doi.org/10.1029/97GL00689.

Wyrtki, K., 1975: El Niño—The dynamic response of the equatorial Pacific Ocean to atmospheric forcing. *J. Phys. Oceanogr.*, **5**, 572–584, https://doi.org/10.1175/1520-0485(1975)005<0572:ENTDRO>2.0.CO;2.

Zhu, X., R. J. Greatbatch, and M. Claus, 2017: Interannual variability of tropical Pacific sea level from 1993 to 2014. *J. Geophys. Res. Oceans*, **122**, 602–616, https://doi.org/10.1002/2016JC012347.